Atmospheric Environment 249 (2021) 118153

Contents lists available at ScienceDirect

Atmospheric Environment

journal homepage: http://www.elsevier.com/locate/atmosenv

Unraveling the diurnal atmospheric ammonia budget of a prototypical convective boundary layer

R.B. Schulte [a,b,*], M.C. van Zanten [b], S. Rutledge-Jonker [b], D.P.J. Swart [b], R.J. Wichink Kruit [b], M. C. Krol [a], W.A.J. van Pul [b], J. Vilà-Guerau de Arellano [a]

[a] Wageningen University & Research, P.O. Box 47, 6700, AA Wageningen, the Netherlands
[b] National Institute for Public Health and the Environment (RIVM), Antonie van Leeuwenhoeklaan 9, 3721, MA Bilthoven, the Netherlands

ARTICLE INFO

Keywords:
Ammonia
Convective boundary layer
Diurnal variability
Modeling. measurements
Budget

ABSTRACT

We investigate diurnal variability of the atmospheric ammonia (NH_3) budget over unfertilized grassland by combining observations with a conceptual atmospheric boundary layer model. Our combined approach of diurnal observations and modeling enables us to identify the contribution of the four governing processes to the NH_3 diurnal cycle: surface-atmosphere exchange, entrainment, advection and chemical gas-aerosol transformations. The observations contain new NH_3 flux and molar fraction measurements obtained using the Differential Optical Absorption Spectroscopy (DOAS) remote sensing technique, eliminating problems related to inlet tubing. Using strict filter criteria, 22 days with clear-sky summer conditions are selected. From this selection, we analyze a single representative day characterized by prototypical convective boundary layer conditions, using the boundary layer model constrained by meteorological observations.

We design two numerical experiments to study the NH_3 diurnal variability and the individual contributions of the processes governing the ammonia budget. These experiments only differ in their representation of the NH_3 surface exchange. First, a fitted function through the observed NH_3 flux is prescribed to the model. In the second numerical experiment, the surface flux is solved following the DEPosition of Acidifying Compounds (DEPAC) parameterization. With a prescribed surface flux, the modeled NH_3 molar fraction closely fits the observations. Two regimes are identified in the NH_3 diurnal cycle: the morning, where boundary layer dynamics dominate the budget through entrainment, and the afternoon, where multiple processes are of importance. A similarly close fit to the observed molar fraction is achieved in the second experiment, but we identify a mismatch between the observed and parameterized NH_3 surface flux. As a result, the model requires an unrealistic budget representation to achieve this close fit, e.g. high free tropospheric NH_3. Our findings on the NH_3 budget, based on integrating modeling and observations, paves the way for future research on the NH_3 surface-atmosphere exchange at the subdaily scales.

1. Introduction

It is well established that excess nitrogen deposition leads to acidification and eutrophication of soils; threatening biodiversity (Bobbink et al., 2003; Erisman et al., 2007, 2013). The European Union has made the conservation of natural habitats, i.e. Natura 2000 areas, an essential objective through the EU Habitats Directive (92/43/EEC) and EU Birds Directive (79/409/EEC). This includes mitigation of the harmful effects of nitrogen deposition. Currently, nitrogen deposition in most Dutch Natura 2000 areas exceed critical loads, leading to the highest administrative court of the Netherlands scrapping the permit system for all projects which include any nitrogen pollution, blocking plans for farm expansions and construction of new homes, roads and airport runways. The high court decision led to economic damage and political and social unrest, known as the Dutch nitrogen crisis. Ammonia (NH_3) plays a key role in this crisis as it accounts for two-thirds of all nitrogen deposition in the Netherlands between 2005 and 2016 (Wichink Kruit and van Pul, 2018). Policies to mitigate the adverse effects of ammonia are supported by several decades of scientific studies on atmospheric ammonia, leading to observational networks, deposition parameterizations and air quality forecasting models (Sutton et al., 2008). However, these studies are mainly focusing on low spatio-temporal resolutions, e.g. monthly to

* Corresponding author. Wageningen University & Research, P.O. Box 47, 6700, AA Wageningen, the Netherlands.
E-mail address: ruben.schulte@wur.nl (R.B. Schulte).

https://doi.org/10.1016/j.atmosenv.2020.118153
Received 4 November 2020; Received in revised form 14 December 2020; Accepted 14 December 2020
Available online 29 December 2020

yearly averages with grids ranging from 1 × 1 km to 50 × 50 km (Simpson et al., 2012; Manders et al., 2017; Matthias et al., 2018; Sauter et al., 2018; Schaap et al., 2008; Schrader et al., 2016, 2018). As a result, surface, dynamic and chemistry processes governing the diurnal evolution of the atmospheric ammonia budget are often simplified or not well captured. This study aims to disentangle the atmospheric ammonia budget by combining observations with a convective boundary layer model at subdaily and local scales.

The atmospheric ammonia budget is studied as a mass balance between the atmospheric molar fraction ("Storage"), sources and sinks. Fig. 1 shows a schematic representation of this budget in an evolving convective boundary layer (CBL), with the four main processes governing the budget: (bi-directional) surface exchange, entrainment of free tropospheric (FT) air, advection and chemical gas-particle transformations. These processes combine multiple disciplines, such as biology and chemistry, and interact on multiple spatio-temporal scales, ranging from stomatal responses of vegetation to NH_3 advection over several kilometers (Farquhar et al., 1980; Sutton et al., 1995; Fowler et al., 1998; Sommer et al., 2009; Shen et al., 2016). Integration of these disciplines and scales is essential for any study concerning atmospheric ammonia, making it a highly complex exercise. It is the novelty of this study that we integrate these four processes via modeling and the maximum use of observations. Observations of ammonia add an additional layer of complexity as the gas tends to "stick" to inlet walls of conventional instruments, causing slow response times, hysteresis and a sensitivity to changes in relative humidity. Additionally, evaporation of ammonium aerosols from filters and the instrument interior leads to further inaccuracies with conventional NH_3 observations (von Bobrutzki et al., 2010; Whitehead et al., 2008). As a result, ammonia concentration and flux measurements at high temporal resolution are scarce.

By analyzing observations over more than 100 days collected over an unfertilized grass field in the Netherlands, we design a case study to identify the contributions of each process to the diurnal variability of the NH_3 budget. The numerical experiments are constrained by observations of a representative single-day Case, characterized by convective boundary layer conditions. The observations include ammonia concentration and flux measurements by a state-of-the-art optical instrument, eliminating the inlet issues typical for conventional NH_3 observations. We set up a two-experiment approach where we first disentangle the ammonia budget based on observations and follow up by evaluating the standard parameterization against the observations at subdaily scales. To this end, we prescribe the observed NH_3 flux to the model in the first numerical experiment. Next, we change the representation of the NH_3 surface exchange in the second experiment by parameterizing the NH_3 flux following the parameterization standard in the Netherlands: DEPosition of Acidifying Compounds (DEPAC) v.3.11 (van Zanten et al., 2010).

2. Methodology

2.1. Meteorological site description

This study focuses on the Veenkampen meteorological site in the Netherlands, located west of Wageningen (51.98° N, 5.62° E) at 4 m above sea level. The site is maintained by Wageningen University & Research and has been in operation since 2011, succeeding the former Haarweg meteorological site which operated from 2001 to the end of 2011 (Calders et al., 2015). The automated weather station provides half-hourly measurements of several meteorological variables, radiation and soil temperature and moisture. An overview of the available measurements can be found at https://met.wur.nl/veenkampen/graphs/cur/ and the data is freely available at https://met.wur.nl/veenkampen/data. The soil at the 17-ha Veenkampen site consists of a clay layer of approximately 1 m over peat. In 2011, the site was sown in with reyegrass and species composition has not been monitored or managed since. The grass has an approximated height of 10 cm and is cut regularly during the growing season (April to September). Fertilization of the site stopped in 1979. Yearly average deposition of NHx, modeled by the Dutch National Institute of Public Health and the Environment at 1 × 1 km resolution (Velders et al., 2014), is about 1000 mol $ha^{-1}year^{-1}$ at the site.

At the northern border of the Veenkampen site, about 50 m from the centerline, reeds up to 1.5 m high are found. The nearest trees are 350 m east of the site. Both the reeds and the trees could impact the turbulent flow at the site for medium to high wind speeds. Neighboring fields are similar in composition, but could differ in nitrogen content as intensive management only stopped some time before 2011. Farms, mostly livestock, are found in all directions, with the closest located about 1.75 km north, 1.20 km east, 1.50 km south and 0.65 km west of the Veenkampen. These nearby farms are likely to contribute significantly to the atmospheric NH_3 concentrations and high deposition at Veenkampen.

To complement the observations at Veenkampen, we support our study with boundary layer height observations from the Ruisdael Observatory at Cabauw (www.ruisdael-observatory.nl). These

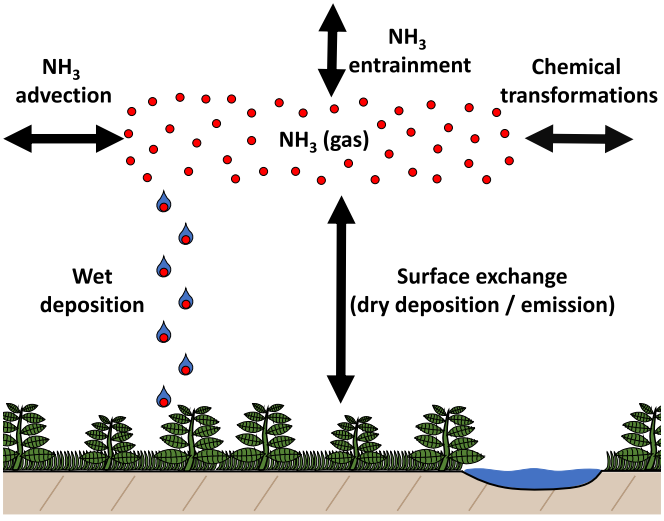

Fig. 1. Schematic representation of the atmospheric ammonia budget.

measurements are taken using a LD40 ceilometer (Vaisala, Bonn, Germany). Additionally, radiosonde measurements from the De Bilt weather station of the Royal Netherlands Meteorological Institute (KNMI) were used. These two locations are located 50 km and 35 km west of Veenkampen.

2.2. Ammonia observations

Ammonia concentration and flux measurements are taken at the Veenkampen by two Differential Optical Absorption Spectroscopy (DOAS) instruments (Volten et al., 2012a). These instruments measure the average NH_3 mass density (ρ_{NH_3}) over a 50 m open path between the instrument and its retroreflector. Two parallel paths are set up above one another at heights of 0.65 m and 2.36 m respectively, referred to as $NH_{3,\ 0.65\ m}$ and $NH_{3,\ 2.36\ m}$. The mass density is calculated from 30-min averaged spectra with a typical standard deviation of 0.15 μg m^{-3} (Volten et al., 2012a). Both DOAS instruments are intercalibrated regularly in the field with special measurements. The instruments are placed in a small building, covered by a smooth man-made hill to minimize flow disturbance, about 30 m in diameter and 3 m high. The setup includes 20 Hz turbulent measurements at 3.2 m from a CSAT3 sonic anemometer (Campbell Scientific Inc., Logan, UT, USA). The anemometer is located in the middle of the path to get the 30-min average turbulent properties representative for the path. This state-of-the-art NH_3 measurement setup is unique in the world and has so far been used in two studies: NH_3 exchange measurements over a corn field (Wichink Kruit et al., 2010a; Volten et al., 2012b) and as part of a surface exchange parameterization validation study over grassland (Schrader et al., 2016).

The ammonia flux (F_{NH_3}) is inferred from DOAS concentration observations by applying the flux-gradient method, following Equation (1).

$$F_{NH_3} = -K_{NH_3}\frac{\partial NH_3}{\partial z} \approx -K_{NH_3}\frac{\Delta NH_{3\ obs}}{\Delta z_{obs}} \tag{1}$$

Here $\frac{\Delta NH_{3\ obs}}{\Delta z}$ is the observed concentration gradient and K_{NH_3} is the eddy diffusion coefficient for NH_3. We parameterize K_{NH_3} similar to the diffusion coefficient of heat, using Monin-Obukhov similarity theory including the stability effects, which depends on the intensity of turbulent mixing resulting from the sonic anemometer observations. K_{NH_3} is determined using Equation (2),

$$K_{NH_3} = \frac{ku_* z}{\varphi_{NH_3}(z/L)} \tag{2}$$

where k is the von Karman's constant (assumed $k = 0.4$), u_* is the observed friction velocity, z is the height above the displacement height d, defined by 2/3 of the canopy height. The atmospheric stability effects are taken into account by $\varphi_{NH_3}(z/L)$, the dimensionless flux-gradient relationship as a function of z/L, where L is the Obukhov length. For the flux-gradient relationships, we use the commonly used Businger-Dyer relationships (Dyer and Hicks, 1970).

To derive F_{NH_3}, we vertically integrate the gradients of Equation (1) to obtain Equation (3).

$$F_{NH_3} = \frac{-u_* k\left(NH_{3,\ 2.36\ m} - NH_{3,\ 0.65\ m}\right)}{ln\left(\frac{z_{2.36\ m}-d}{z_{0.65\ m}-d}\right) - \Psi_{NH_3}\left(\frac{z_{2.36\ m}-d}{L}\right) + \Psi_{NH_3}\left(\frac{z_{0.65\ m}-d}{L}\right)} \tag{3}$$

We use $z_{0.65\ m}$ and $z_{2.36\ m}$ to represent the height of the NH_3 concentration measurements, with a displacement height d of 0.07 m, and Ψ_{NH_3} represents the integrated flux-gradient relationship for ammonia. For the latter, we assume the relation for ammonia to be equal to those of water vapor and heat, following Ψ_h derived by Paulson (1970), based on the Businger-Dyer flux-gradient relationships for unstable conditions ($z/L<0$). For stable conditions, Ψ_h is derived by Beljaars and Holtslag (1991).

Note that DOAS observes the mass density of ammonia (ρ_{NH_3}), in μg m^{-3}. We convert the DOAS observations following Equation (4) as the model solves chemical species as molar fraction.

$$NH_{3,v} = \frac{V_{STP}}{M_{NH_3}}\frac{T}{T_{STP}}\frac{p_{STP}}{p}\rho_{NH_3} \tag{4}$$

Here $NH_{3,v}$ is the NH_3 molar fraction in ppb, T is the observed temperature and p is the observed pressure. The other variables are constants for the molar mass of NH_3 ($M_{NH_3} = 17.03$ kg $kmol^{-1}$), volume of air at Standard Temperature and Pressure ($V_{STP} = 22.4$ m^3), standard temperature ($T_{STP} = 273.15$ K) and standard pressure ($p_{STP} = 101.325$ 10^3 Pa). In this paper, we show the NH_3 flux in μg $m^{-2}s^{-1}$ for the sake of interpretation and consistency with literature.

2.3. Data filtering

We apply several filter criteria to the observations, shown in Table 1. As we are interested in the interaction between processes spanning various spatio-temporal scales, we aim to study the budget under meteorological conditions in which the local land-atmospheric conditions are dominant. Therefore, we focus in this study on the ammonia budget under typical clear-sky summer conditions, i.e. the months of May to August.

We first filter the DOAS observations to ensure high quality measurements. To this end, we only consider observations from 2013, because of the high data availability and quality compared to other years. Intercalibration measurements are excluded as well, as no NH_3 flux can be inferred from these observations. A minimum DOAS signal intensity is required to assure high quality concentration measurements. Note that these optical measurements are sensitive to meteorological conditions which can obstruct the open path and lead to a significant reduction of signal intensity, e.g. rain or (shallow) fog events which are particularly common in the Netherlands (Izett et al., 2018). Furthermore, we filter out NH_3 concentration measurements with a standard deviation over 0.3 μg m^{-3} for concentrations below 20 μg m^{-3}, or over 1.5% of concentrations over 20 μg m^{-3}. After these DOAS quality filters, 47% of all observations from May to August remain.

Secondly, we filter the observations for the meteorological condi-

Table 1
Filter criteria for clear-sky summer conditions, applied to meteorological and DOAS NH_3 observations for the months May up to and including August of 2013.

Filter		criterion	Acceptance [%]	Acceptance [hours]
Unfiltered observations		–	100%	2952
DOAS intercalibration		*Exclude*	74%	2172.5
DOAS signal intensity (Xe)		Xe > 15,000 counts	47%	1402
$NH_{3\ obs}$ error:	$NH_{3\ obs} < 20$ μg m^{-3} $NH_{3\ obs} \geq 20$ μg m^{-3}	$\sigma_{NH_3} < 0.3$ μg m^{-3} $\sigma_{NH_3} < 0.015\ NH_{3\ obs}$	47%	1384
Net radiation (Q_n)		Q_n>0	30%	888
Atmospheric stability		z/L<0	21%	606.5
Sunshine duration $t_{sunshine}$		$t_{sunshine}$>1350s/1800s	9%	267

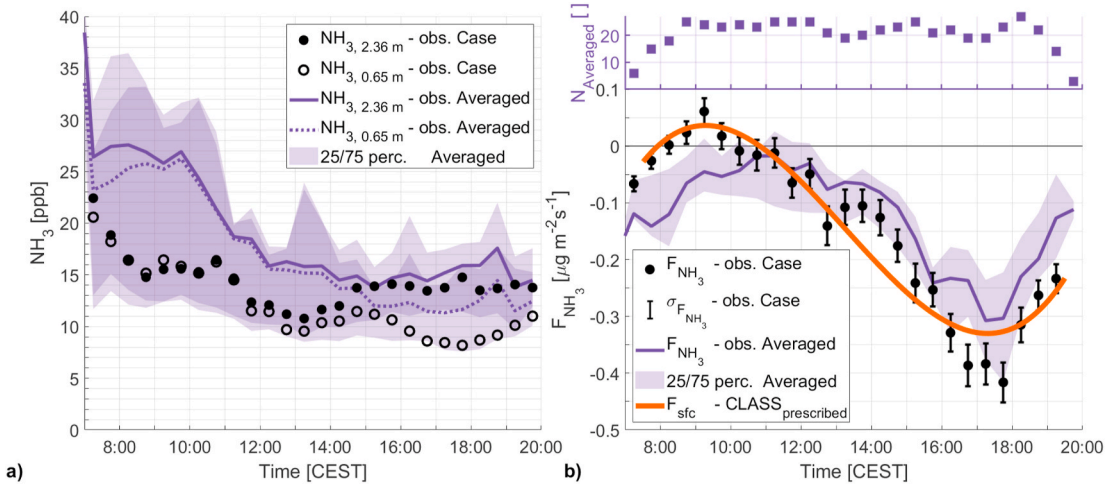

Fig. 2. The diurnal variability of the ammonia molar fraction observations (a) and ammonia surface flux (b). Uncertainties for the molar fraction observations are smaller than the symbols. Case observations of July 8, 2013 are shown in black and the multi-day Averaged Summer Day observations are shown as a purple line, with their respective 25/75 percentile shown as purple shading. Atop the NH_3 flux, we display the N number of observations over which the average is taken to construct the Averaged Summer Day. A third degree polynomial fit to the Case NH_3 flux, used in the $CLASS_{prescribed}$ experiment, is shown in orange. (For interpretation of the references to colour in this figure legend, the reader is referred to the Web version of this article.)

tions required to perform this case-study. We characterize typical summer conditions by a convective boundary layer and clear skies. Three criteria are set up to find observations under these conditions. We first filter the data for convective conditions with two criteria: positive net radiation ($Q_n > 0$) and a negative Monin-Obukhov stability parameter ($\frac{z}{L} < 0$). The remaining 21% of the data is filtered for clear-sky conditions, using the sunshine duration observations of a CSD3 Sunshine Duration Sensor (Kipp & Zonen, Delft, Netherlands) at Veenkampen. Here, we apply a minimum sunshine duration of 22.5 min per 30 min. After filtering, 9% of the available observations remain, i.e. 267 h. When one considers a 12 period hours per day for which these criteria are met, this translates to about 22 days of observations.

2.4. Representing a prototypical convective boundary layer

The selection of the single day for the case-study, representative of typical summer day conditions, requires one additional criterium: data availability from sunrise to sunset ($Q_n > 0$), i.e. completeness. Out of the remaining four complete days (not shown), July 8, 2013 is selected as our Case, because of the low variability in wind direction (not shown) and because the main surface and boundary-layer characteristics follow a representative situation of convective summer conditions. Case observations of boundary layer height (h), potential temperature (θ) and specific humidity (q) are discussed in Section 3.1. The observed NH_3 molar fraction and surface flux are shown in black in Fig. 2. The observed diurnal variability of the molar fraction of our Case is characterized by high values in the early morning, followed by a rapid decrease. The molar fraction temporarily levels with a possible local maximum between 8:00 and 11:00 CEST, after which the molar fraction rapidly decreases again. Between 13:00 and 19:00 CEST, the molar fraction stabilizes at approximately 12 ppb. Note that the vertical NH_3 molar fraction gradient significantly increases between 12:00 and 19:00 CEST.

The Case observed NH_3 flux in Fig. 2b, where a negative flux represents deposition, also shows a clear distinction between the morning and afternoon. From 7:00 to 12:00 CEST, both low deposition and low emission are observed. As a result of the increasing NH_3 gradient, a large negative flux is found between 12:00 and 19:00 CEST, peaking around 17:30 CEST.

In addition to our single day Case, we find this observed diurnal variability in multiple convective conditions. In short, we analyze 267 h of filtered data to calculate the average diurnal variability for clear-sky summer days. The NH_3 molar fraction and surface flux of this representative "Averaged Summer Day" (purple lines) are shown in Fig. 2. Here we find that the Case observed molar fraction (black) is within the 25 and 75 percentile of the Averaged Summer Day (purple shading). Note that, while the Case observations are in the lower end of the spread, both the Case and the Averaged Summer Day follow a similar diurnal pattern. In Fig. 2a, a strong decrease in the NH_3 molar fraction in the morning, as well as a clear vertical gradient between 12:00 and 19:00 CEST, are found for both sets of observations. Considering the NH_3 surface flux in Fig. 2b, the Case observed flux is shown to be partly outside the rather small 25/75 percentile spread of the Averaged Summer Day. Again, the same subdaily pattern of low deposition/emission in the morning and high deposition in the afternoon is found for both the sets of observations. We therefore conclude that the results presented in this study can be generalized to cloudless convective conditions, characterized by weak large-scale forcing.

2.5. Model description

The Chemistry Land-surface Atmosphere Soil Slab (CLASS) model (Vilà-Guerau de Arellano et al., 2015) is a convective boundary layer model used to support the interpretation of the observations. With CLASS, we aim to integrate the processes that drive the diurnal variability of NH_3 concentration and flux. We represent and connect all

relevant processes to the boundary layer ammonia budget of Fig. 1 in order to identify their respective influences.

CLASS solves the surface-atmosphere exchange using five interacting layers: the mixed-layer, the atmospheric surface layer, the surface, the top soil layer and the deep soil. It is in the well-mixed layer that the model describes the state conserved boundary layer variables, which include meteorological variables and chemically active species (Ouwersloot et al., 2012). The surface layer, the bottom 10% of the CBL, connects the mixed-layer to the surface. Parameterization of surface characteristics is done at the infinitesimally thin surface. Using moisture exchange (latent heat) as an example, three parallel paths are parameterized: soil evaporation, liquid water (dew) evaporation and vegetation evapotranspiration. The latter follows the A-g_s approach (Ronda et al., 2001), where the A represents the photosynthesis process and g_s represents the stomatal conductance of carbon dioxide/water at canopy level. While the top soil layer also directly interacts with the atmosphere, the deep soil layer mainly acts as reservoirs of heat and moisture, only interacting with the top soil layer. These layers are coupled, i.e. actively solved by the model and only require initial values.

CLASS assumes the boundary layer to be well-mixed, requiring the same well-mixed conditions for which we filter the observations in Section 2.3. It allows us to describe atmospheric and chemical variables as a bulk model in which quantities are approximately constant with height without losing representativeness.

In order to describe any quantity $\psi(t,x,y,z)$ as a bulk variable, several assumptions are required. First, we assume the CBL flow to have horizontally homogeneous properties for all variables: $\psi(t,x,y,z) \approx \psi(t,z)$. Secondly, the mean vertical velocity within the CBL is assumed to be zero: $\overline{w} \approx 0$, i.e. we only account for the vertical turbulent flux ($\overline{w'\psi'}$). Finally, there is the assumption that thermodynamic variables are well mixed in convective conditions and are therefore approximately constant with height. It allows us to represent any variable in the whole vertical domain with a single value, the bulk value, by integrating with height: $\psi(t,z) \approx \langle\psi(t)\rangle$. With these assumptions, we can describe the temporal evolution of $\langle\psi\rangle$ with Equation (5).

$$\underbrace{\frac{\partial\langle\psi\rangle}{\partial t}}_{Storage} = \underbrace{\frac{1}{h}(\overline{w'\psi'})_s}_{SFC} - \underbrace{\frac{1}{h}(\overline{w'\psi'})_e}_{ENT} + \underbrace{\langle adv\rangle}_{ADV} + \underbrace{\langle chem\rangle}_{CHEM} \tag{5}$$

Here, $(\overline{w'\psi'})_s$ and $(\overline{w'\psi'})_e$ describe the turbulent fluxes at the surface and entrainment at the top of the CBL. Additional changes to $\langle\psi\rangle$ can result from advection (ADV) and chemical transformations (CHEM). Other sources and sinks can be added to Equation (5) similar to these last two terms. In order to resolve the evolution equation, we require parameterization of the turbulent entrainment flux $(\overline{w'\psi'})_e$ (Equations (6) and (7)).

$$(\overline{w'\psi'})_e = -w_e\Delta\psi = \left(\frac{\partial h}{\partial t} - w_s\right)\Delta\psi \tag{6}$$

$$\frac{\partial\Delta\psi}{\partial t} = \gamma_\psi\left(\frac{\partial h}{\partial t} - w_s\right) - \frac{\partial\langle\psi\rangle}{\partial t} \tag{7}$$

In Equations (6) and (7), w_e represents the entrainment velocity, i.e. the exchange velocity between the CBL and the free troposphere (FT), w_s represents the subsidence velocity resulting from large scale synoptic weather, Δ_ψ represents the infinitely small inversion layer at the top of the CBL: $\Delta_\psi = \psi_{FT} - \psi_{CBL}$. Finally γ_ψ represents the lapse rate of ψ. The entrainment velocity is related to the growth/decline of the CBL ($\frac{\partial h}{\partial t}$), which specifically depends on the virtual potential temperature (θ_v). This is shown in Equation (8), where β is the ratio of the entrainment to the surface buoyancy flux, for which we use β = 0.2 as closure assumption (Stull, 1988).

$$\frac{\partial h}{\partial t} = \frac{\beta(\overline{w'\theta_v'})_s}{\Delta\theta_v} + w_s \tag{8}$$

With these four equations, the CLASS model is used to integrate the evolution with time of atmospheric ammonia ($\psi = NH_3$), or any meteorological, chemical or tracer variable.

2.6. Research design

The combination of the CLASS model and the DOAS NH_3 observations allows us to design a two-experiment approach to study the diurnal variability of the ammonia budget and the individual contributions of the four governing processes of Equation (5). These numerical experiments only differ in their representation of the surface exchange process (SFC). In the first experiment, named $CLASS_{prescribed}$, we fully control the surface exchange by prescribing the NH_3 surface flux to the model (F_{sfc}) following a third order polynomial fit to the DOAS observed surface flux (F_{NH_3}), shown in orange in Fig. 2b. Here the flux is decoupled from the surface conditions. This experiment allows us to quantify the contributions of each process to the temporal evolution of $\langle NH_3\rangle$, i.e. changes in the NH_3 storage term of Equation (5).

In the second numerical experiment, we release our control on the NH_3 surface exchange and couple the surface flux to the diurnal variability of the state variables. For this purpose, the model uses the DEPosition of Acidifying Compounds (DEPAC) v.3.11 parameterization (Wichink Kruit et al., 2010b; van Zanten et al., 2010). With this second experiment, named $CLASS_{DEPAC}$, we aim to evaluate the performance of the parameterization against the DOAS observations.

The representations of the remaining three budget processes are the same for both experiments. Entrainment (ENT) depends on boundary layer growth ($\frac{dh}{dt}$) and the free tropospheric ammonia molar fraction ($NH_{3,\,FT}$). While $\frac{dh}{dt}$ is constrained by ceilometer observations at Cabauw, $NH_{3,\,FT}$ requires estimation, as observations are lacking. Similarly, advection (ADV) requires estimation due to a lack of observations. In this study we prescribe advection to CLASS as a constant forcing term, as a first order estimate. Finally, chemical transformations (CHEM) are solved by implementing the ISORROPIA version 2 thermodynamic equilibrium model (Fountoukis and Nenes, 2007). ISORROPIA2 provides the equilibrium molar fractions in the ammonium-nitrate-sulfate system, which are sensitive to the atmospheric temperature and relative humidity. We account for the equilibrium time by calculating the new molar fraction following Equation (9).

$$\frac{\partial\langle NH_3\rangle}{\partial t} = \frac{NH_{3,\,eq} - \langle NH_3\rangle}{\tau_p} \tag{9}$$

Here, $NH_{3,\,eq}$ is the equilibrium molar fraction from ISORROPIA2 in ppb and τ_p is the partitioning time scale, set to 1800 s (30 min) (aan de Burgh et al., 2013; Barbaro et al., 2015; Guo et al., 2018). We initialize our model with a total amount of ammonia/ammonium, nitrate and sulfate in the boundary layer by only initializing these species in the gas phase following aan de Burgh et al. (2013), shown in Table 2 of Appendix B. At the very first time step (not shown), the model finds the gas-aerosol equilibrium. For the remaining simulation time, both

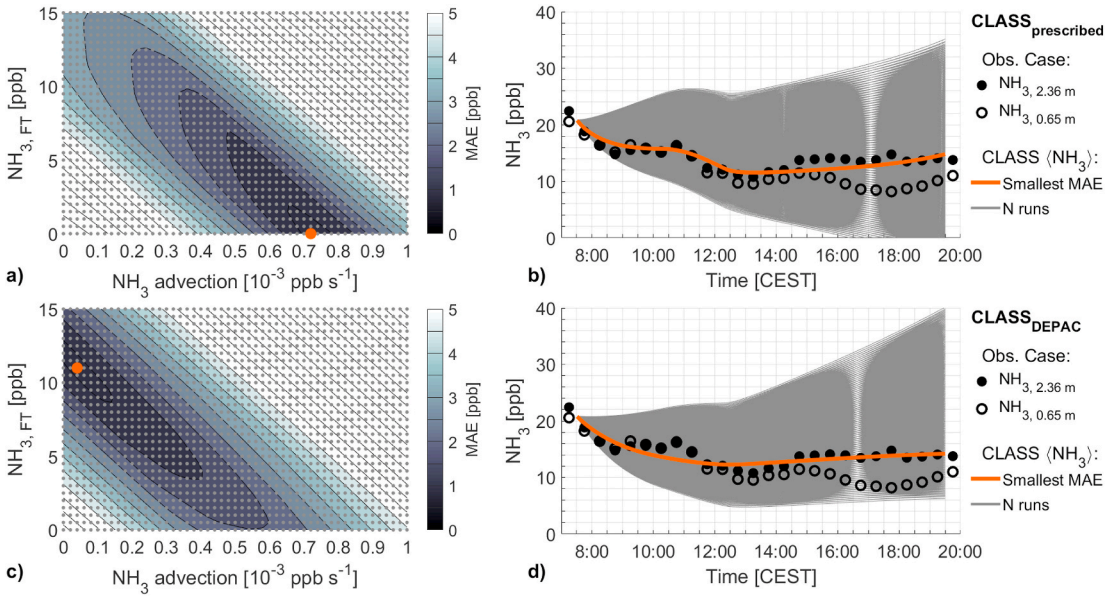

Fig. 3. The results of the systematic estimation of the initialization of $NH_{3,\ FT}$ and advection for the $CLASS_{prescribed}$ experiment (a and b) and $CLASS_{DEPAC}$ experiment (c and d). The sensitivity of $\langle NH_3 \rangle$ to these variables, by ways of the MAE with respect to the observed $NH_{3,\ 2.36\ m}$, is shown left (a and c). The modeled $\langle NH_3 \rangle$ of each individual combination is shown right (b and d). Results of the individual runs are shown in grey, with the smallest MAE combination shown in orange. The experiments are initialized with the $NH_{3,\ FT}$ and advection resulting in the smallest MAE. (For interpretation of the references to colour in this figure legend, the reader is referred to the Web version of this article.)

gaseous NH_3 and NH_4^+ aerosols are simulated and the partitioning time is applied.

We perform a systematic estimation of the initial conditions of $NH_{3,\ FT}$ and advection, by studying the sensitivity of the modeled mixed layer molar fraction ($\langle NH_3 \rangle$) to these two variables. We vary $NH_{3,\ FT}$ and advection and compare the modeled $\langle NH_3 \rangle$ to the observed molar fraction at 2.36 m ($NH_{3,\ 2.36\ m}$) by calculating the Mean Absolute Error (MAE) between the two. The combination of $NH_{3,\ FT}$ and advection with the smallest MAE will be used to initialize the CLASS model. In doing so, we aim to find the best initial conditions in absence of measurements. The process is repeated for both the $CLASS_{prescribed}$ and $CLASS_{DEPAC}$ experiment, as any change in the representation of the surface exchange could potentially lead to a different result. Fig. 3 shows both the resulting MAE (left) and each resulting $\langle NH_3 \rangle$ (right) for both the $CLASS_{prescribed}$ (a and b) and the $CLASS_{DEPAC}$ (c and d) experiment. These results are interpreted in Sections 3.2 and 3.3. The complete initialization of both $CLASS_{prescribed}$ and $CLASS_{DEPAC}$ can be found in Table 2 of Appendix B.

3. Results

3.1. Model performance

Fig. 4 shows the observed and modeled boundary layer height (h), specific humidity (q), potential temperature (θ) and modeled entrainment velocity (w_e) between 9:30 CEST and 19:30 CEST, i.e. convective conditions ($Q_n > 0$). It shows that CLASS represents these main characteristics of the boundary-layer dynamics well, as the model output closely resembles the observations.

We take a closer look at the boundary layer height in Fig. 4a. To achieve a good representation of the boundary layer growth, the model is initialized with three atmospheric regimes based on both radiosonde and ceilometer observations: the initial inversion layer at the start of the simulation, called the transitional layer, the residual layer and the free troposphere. The transitions between each regime is highlighted with A at 400 m and with B at 700 m. Each regime is characterized by its own lapse rate for heat (γ_θ) and moisture (γ_q), which can be found in Table 2. As a result, each regime is characterized by a different rate of boundary layer growth. This is best visualized by the entrainment velocity (w_e) from Equation (6), shown in Fig. 4c. Here we find a rapid velocity increase from the moment h reaches the residual layer at 400 m (A). Boundary layer growth, and entrainment velocity with it, slows down when h reaches the free troposphere at 700 m (B). These different regimes allow us to make a distinction between the morning with an actively developing boundary layer until 12:21 CEST (B) and the afternoon where boundary layer growth slows down.

When inspecting the modeled 2 m potential temperature in Fig. 4b, we see that it follows the observations quite well. The model underestimates the maximum 2 m θ by 2 K when compared to Veenkampen observations and overestimates the more western Cabauw observations by 1 K. A temperature difference between the two locations is expected, as the west of the Netherlands is generally cooler in summer due to the influence of the North Sea. Overall, θ is well represented by the model, considering that h is constrained by observations at Cabauw and De Bilt, west of Veenkampen.

Moisture acts on a more local scale than temperature, as it highly depends on the local vegetation and soil conditions. This is clearly shown by the observed specific humidity at Veenkampen and Cabauw in Fig. 4d. While the pattern of the temperature is similar for both locations, the q-humidity observations only agree until 11:00 CEST, after which the specific humidity decreases at Veenkampen. Note that our boundary conditions lead to a drying of the CBL driven by entrainment. A sharp decrease of over 1 g kg^{-1} in q is observed at 18:00 CEST, as well as a collapse of the CBL at 18:30 CEST. These features are not well

reproduced by the model as they are a likely a result of changes in synoptic weather, e.g. a sea breeze effect or a weak cold front as seen on the synoptic weather map (https://www.knmi.nl/nederland-nu/klimatologie/daggegevens/weerkaarten). The disagreement between the modeled and the observed specific humidity can have a small impact on the chemical gas-aerosol equilibrium, as it is sensitive to changes in relative humidity. The disagreement can also have a minor impact on the magnitude of the parameterized NH_3 flux, as DEPAC follows a resistance based modeling approach with surface resistances being sensitive to changes in humidity (Appendix A).

3.2. Experiment 1: the diurnal variability of atmospheric NH_3

The satisfactory agreement between meteorological observations and modeling enables us to move on and model the ammonia budget following Equation (5). Fig. 5 shows the modeled and observed ammonia molar fraction (a), the modeled and observed NH_3 flux (b) and the changes in the modeled molar fraction with time of the $CLASS_{prescribed}$ experiment (c) and the $CLASS_{DEPAC}$ experiment (d). Fig. 5a shows that the modeled molar fraction ($\langle NH_3 \rangle$) closely follows the observations for the $CLASS_{prescribed}$ experiment (solid orange), where the surface flux is prescribed as shown in solid orange in Fig. 5b. We place special emphasis on the temporarily leveling of the molar fraction in the observations between 9:00 CEST and 11:00 CEST, as it is a distinct feature of the diurnal ammonia cycle that is well captured by $CLASS_{prescribed}$ and will be discussed later.

$CLASS_{prescribed}$ is initialized with low $NH_{3,\ FT}$ and high advection, as shown in Fig. 3a. The best fit to the top DOAS observations ($NH_{3,\ 2.36\ m}$), with an MAE of 0.87 ppb, is achieved with $NH_{3,\ FT} = 0.00$ ppb and ADV $= 0.72\ 10^{-3}$ ppb s^{-1}. Such low free tropospheric molar fraction is in line with the findings of Tevlin et al. (2017), who observed that ammonia molar fractions rapidly decreases with height just above the boundary layer in both tower and aircraft observations. While no observations are available on advection, a significant positive contribution is in line with our expectations for unfertilized grass-land surrounded by agricultural activities. Large horizontal molar fraction gradients have been observed over only 1 km from sources (Fowler et al., 1998; Sommer et al., 2009; Shen et al., 2016). However, the horizontal gradient corresponding to the modeled advection, estimated by dividing ADV by the average 10 m wind speed (3.8 m s^{-1}, not shown), is low at 0.19 ppb km^{-1}. This indicates that, even though advection appears to play a significant role in the NH_3 budget, the modeled advection most likely represents a background concentration.

With $CLASS_{prescribed}$, we are able to identify the contribution of the four processes governing the NH_3 budget at the diurnal scale (Fig. 1 and Equation (5)). For the $CLASS_{prescribed}$ experiment, these contributions are visualized in Fig. 5c, which shows changes in ammonia with time, where negative/positive values represent a decrease/increase in atmospheric ammonia, i.e. a sink/source. When analyzing the overall change in the modeled ammonia molar fraction, i.e. "Storage" in equation (5), a distinction between the morning and the afternoon can be made, based on boundary layer dynamics. We use the moment that boundary layer growth begins to stabilize as the start of the afternoon, marked by the decrease of w_e at 12:21 CEST (B). In the morning, the negative values for the Storage term in Fig. 5c indicate decreasing $\langle NH_3 \rangle$, as shown in Fig. 5a. In the afternoon, the positive values indicate an increasing $\langle NH_3 \rangle$. Note that values close to zero are found in Fig. 5c, which coincide with the distinct leveling of the morning molar fraction.

In the morning, until 12:21 CEST, entrainment (ENT) has the largest contribution the ammonia budget. The same can be found in Fig. 6a, which shows the averaged contribution of each process in the morning (from 7:30 CEST to 12:21 CEST) in ppb h^{-1}. Here, ENT is the largest sink of NH_3, with -4.28 ppb h^{-1}, being the main cause of the Storage reduction of -1.80 ppb h^{-1}. Advection (ADV) is the largest source of NH_3 in the morning, adding 2.60 ppb h^{-1} to the budget. Both the surface exchange (SFC) and chemical transformations (CHEM) are shown to only play a small role in the morning budget. Note that entrainment is distinctly shaped as a result of its relation to the entrainment velocity, w_e (Equation (6)). The local absolute minimum and maximum of ENT coincide with the local minimum and maximum of w_e in Fig. 4c, highlighted by A and B in both Figs. 4 and 5. Both the magnitude of ENT and strong visual similarities with the Storage term indicate that entrainment dominates the morning budget.

By analyzing Fig. 5c, we can explain the distinct leveling of the NH_3 molar fraction around 10:00 CEST. This distinct feature is a result of changes in the surface exchange and entrainment. While SFC mainly acts as a sink of ammonia by means of deposition, emission is observed in the morning between 8:00 and 11:00 CEST, making the surface exchange a temporary source of NH_3. Additionally, entrainment temporarily weakens around this time, with a local absolute minimum around 10:20 CEST highlighted by A. This weakening of ENT is a result of a slowdown of the boundary layer growth and the rapid decrease of ΔNH_3 (not shown) with decreasing $\langle NH_3 \rangle$ in the early morning. The combination of these two processes are temporarily in balance with the constant

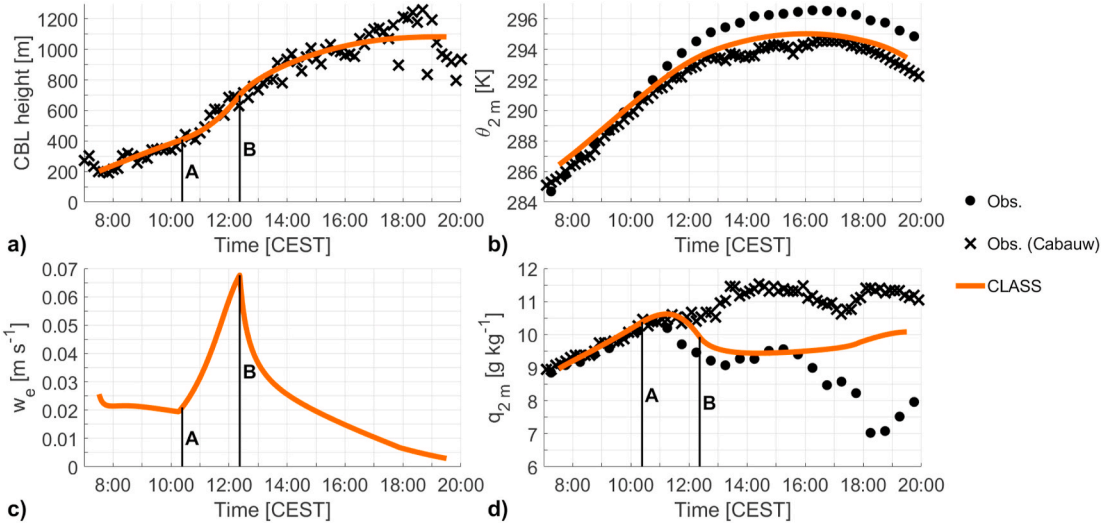

Fig. 4. The Case observed (black) and modeled (orange) diurnal cycle of the CBL height (a), potential temperature (b), entrainment velocity (c) and specific humidity (d). Highlighted are the moments the boundary layer height reaches the top of the transitional layer (A) and residual layer (B). (For interpretation of the references to colour in this figure legend, the reader is referred to the Web version of this article.)

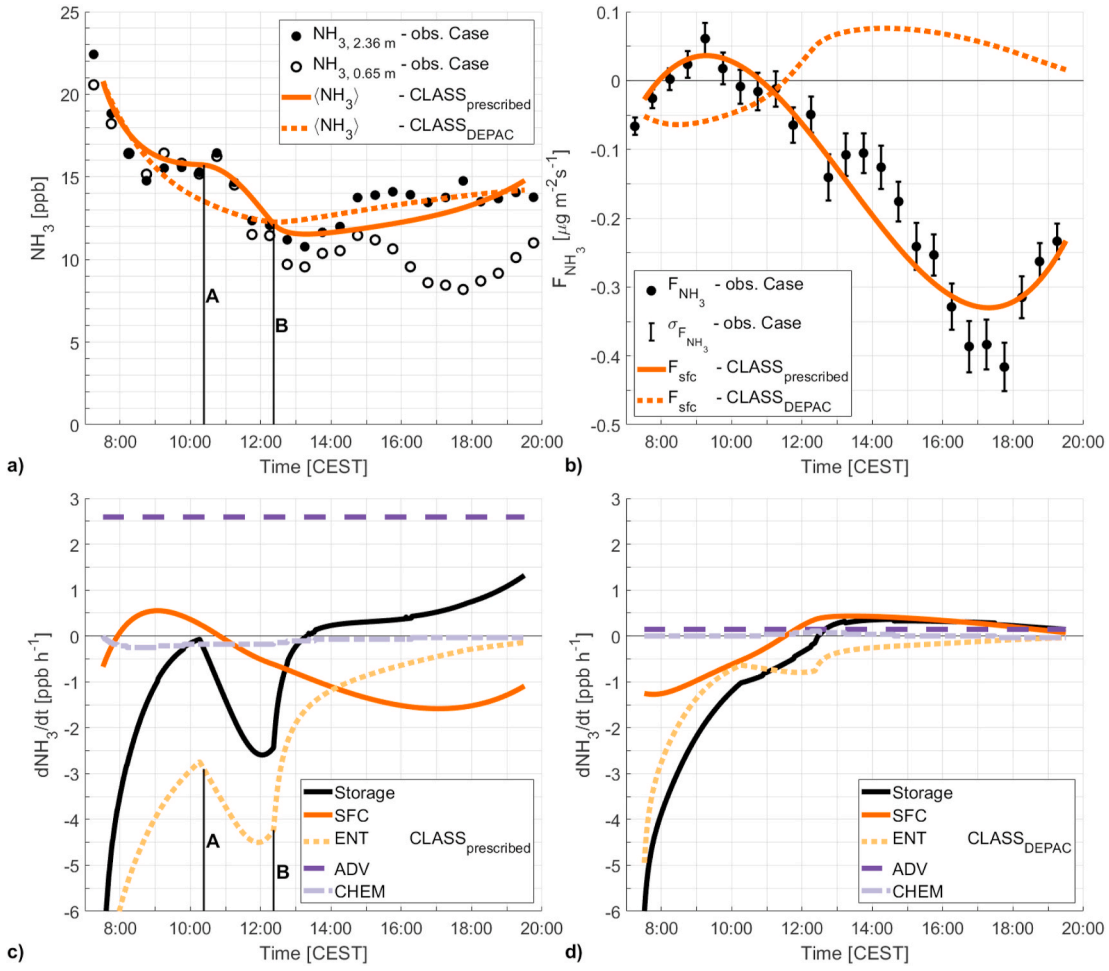

Fig. 5. The diurnal variability of the observed (black) and modeled (orange) NH_3 molar fraction (a), the observed (black) and modeled (orange) NH_3 surface flux (b) and the contributions of each of the four governing processes to the change in modeled NH_3 molar fraction (Storage) for the $CLASS_{prescribed}$ (c) and $CLASS_{DEPAC}$ (d) experiments. The results of the $CLASS_{prescribed}$ experiment are shown as a solid orange line in (a) and (b), with the $CLASS_{DEPAC}$ results shown as a dotted orange line. Highlighted in (a) and (c) are the moments the boundary layer height reaches the top of the transitional layer (A) and residual layer (B). (For interpretation of the references to colour in this figure legend, the reader is referred to the Web version of this article.)

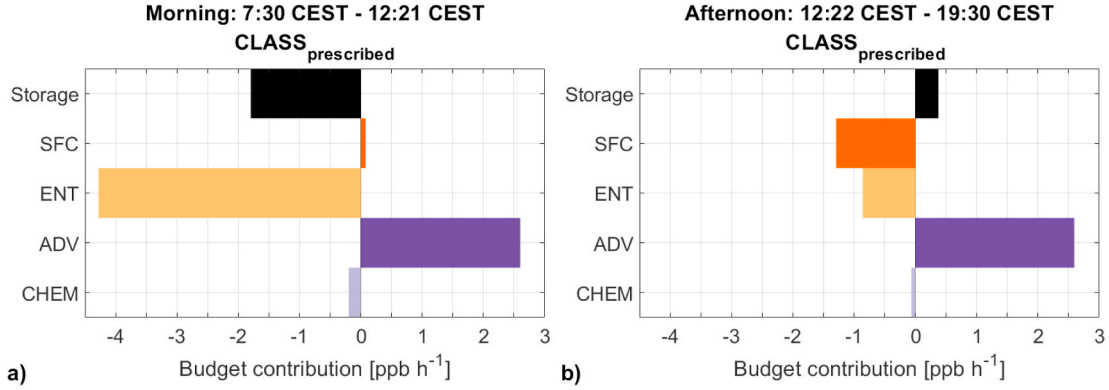

Fig. 6. The individual contributions of each governing process (Equation (5)) to the changing NH_3 molar fraction (Storage) of the $CLASS_{prescribed}$ experiment, averaged over the morning (7:30–12:21 CEST) and afternoon (12:22–19:30 CEST) regimes.

advection, resulting in the leveling of the NH_3 molar fraction.

In the afternoon, from 12:22 CEST to 19:30 CEST, several processes play an important role in the variability of the NH_3 molar fraction. Fig. 5c shows that the contribution of ENT decreases, caused by the slowdown of the boundary layer growth. From 14:00 CEST, SFC becomes the largest sink as the observed deposition peaks in the afternoon. Advection remains the largest, and now only, source of ammonia, as shown in both Figs. 5c and 6b, with a contribution of 2.60 ppb h^{-1} to the budget. Advection is only partly compensated by the surface exchange and entrainment, which contribute −1.29 and −0.86 ppb h^{-1}, respectively. This results in a small increase in $\langle NH_3 \rangle$ (Storage) of 0.38 ppb h^{-1} on average. Similar to the morning, chemical transformations have a negligible contribution, due to the abundance of ammonia and the high temperature, hampering significant transfer of gaseous NH_3 to aerosols.

3.3. Experiment 2: the impact of the NH_3 surface exchange on the diurnal variability

Next, we repeat the previous numerical experiment, but we now release our control on surface exchange. Here, the ammonia surface flux is coupled to the atmospheric diurnal variability, similar to heat and moisture, following the DEPAC parameterization. In short, DEPAC solves the NH_3 surface flux following resistance modeling, where resistances are placed between the atmospheric molar fraction and a canopy compensation point (χ_c), i.e. the canopy internal NH_3 molar fraction (Wichink Kruit et al., 2010b; van Zanten et al., 2010). Two paths are defined for exchange over grassland: the stomatal and external leaf path. Their path-specific resistances and compensation points are parameterized following DEPAC. A full description of this parameterization for grassland is found in Appendix A.

Fig. 5a shows that $\langle NH_3 \rangle$ of the $CLASS_{DEPAC}$ experiment closely follows the observed molar fraction. Here, the model fits the observations closely in the afternoon, but it is unable to capture the distinct leveling off in the morning. Despite the differences, the performance of the two experiments appears to be similar, with an MAE of 0.91 ppb for $CLASS_{DEPAC}$ compared to 0.87 ppb for $CLASS_{prescribed}$.

Fig. 5b shows that the parameterized surface flux (F_{sfc}) of the $CLASS_{DEPAC}$ experiment does not match the observed F_{NH_3}, with F_{sfc} being different in both magnitude and sign. This change in the surface exchange leads to different representations of the other processes, as we tune advection and $NH_{3,\ FT}$ following our systematic estimation of the initial conditions for the model. $CLASS_{DEPAC}$ is initialized with a high free tropospheric molar fraction, $NH_{3,\ FT} = 11.0$ ppb, and low advection, ADV = 0.04 10^{-3} ppb s^{-1} (Fig. 3c). The impact of the new SFC on the other processes of the $CLASS_{DEPAC}$ experiment is presented in Fig. 5d, showing the strongly reduced advection and weaker entrainment compared to the first numerical experiment. An $NH_{3,\ FT}$ that is similar in magnitude as the observed afternoon molar fraction does not match the observations by Tevlin et al. (2017) and seems unrealistic, since there are no sources of NH_3 outside the boundary layer. Even though the low advection also does not match our expectations, we cannot rule this out as a realistic possibility due to the lack of observations on the process. Based on the mismatch between the observed F_{NH_3} and parameterized F_{sfc}, the unrealistic $NH_{3,\ FT}$ and the unexpected low advection, we conclude that the $CLASS_{DEPAC}$ experiment does not realistically reproduce the atmospheric ammonia budget at the temporal resolution of this study.

Our main explanation for the disagreement on the parameterized F_{sfc} and the observed F_{NH_3} concerns the parameterization of the stomatal compensation point (χ_{stom}) in DEPAC. The contribution of the stomatal path increases in the afternoon as the resistance of the external leaf path increases with decreasing relative humidity (Equation (15) of Appendix A). Additionally, the stomatal compensation point is related to (leaf) surface temperature, increasing χ_{stom} with the increasing temperatures. In the afternoon, this leads to an increasing canopy compensation point (χ_c), with temperatures being high and relative humidity being low. Note that F_{sfc} is proportional to the difference between $\langle NH_3 \rangle$ and χ_c. As a result, the parameterized surface flux will always give weak deposition or emission in the afternoon and a deposition peak in the morning, under clear sky convective conditions.

4. General discussion

4.1. Derivation of the NH_3 surface flux from observations

The DOAS setup shows high potential as an optical system to observe the ammonia concentration and flux, therefore eliminating the inlet issues typical of conventional NH_3 observations. However, further developments are recommended to improve the quality of the DOAS gradient measurement. The main challenge with this setup is the need for intercalibration of the two sensitive DOAS instruments in the field. The aim of this intercalibration is to match the zero-level and the span of both instruments to an accuracy that the small concentration differences from dry deposition can be observed. The current process requires manual realignment of the two DOAS instruments with respect to their retroreflectors. When manually switching back to the flux measurement mode, there still appears to be unresolved issues that could prevent maintaining the zero-offset between the instruments that was just obtained. As a result, there may currently still be an unknown fixed offset between the two instruments. It is therefore possible that the fluxes presented in this study are a minor overestimation or underestimation of the actual NH_3 surface exchange.

Inferring fluxes using the flux-gradient method requires several assumption with respect to the surface layer, chemical reactions and horizontal homogeneity. Vilà-Guerau de Arellano et al. (1993) showed for the NO-O_3-NO_2 system that the flux-gradient relationships become more complex when phase transitions and chemical reactions occur at time scales comparable to that of turbulence, which are typically around 15–30 min under diurnal conditions (aan de Burgh et al., 2013; Vilà-Guerau de Arellano et al., 2015). The gas-particle interactions of ammonia, particularly with ammonium nitrate, can indeed lead to a divergence of the turbulent diffusion flux. These interactions are related to the temperature and relative humidity, which do have a near-surface vertical gradient. During the day, these gradients could potentially lead to outgassing of NH_3 from volatile aerosols close to the surface (Nemitz et al., 2004; aan de Burgh et al., 2013). Nemitz et al. (2004) concluded that a flux underestimation of 0.02 μg $m^{-2}s^{-1}$ could be representative for Dutch grassland during daytime. We expect this underestimation for our case study to be small, as nearly all ammonium nitrate aerosols are expected to have evaporated due to the high temperatures. When inferring fluxes using the flux-gradient method, one could estimate, and possibly correct for, this effect by observing temperature and humidity at the individual measurement heights. These new observations can be combined with a thermodynamic equilibrium model, e.g. ISORROPIA2, to calculate a potential molar fraction gradient resulting from NH_3 gas-aerosol interactions.

Additionally, nearby obstacles could disrupt the turbulent flow of air and, depending on wind speed and direction, affect the horizontal homogeneity of the observed gradient as a result, e.g. reeds (Section 2.1). Such disruptions are especially relevant for the DOAS measurement

setup, as the ammonia molar fractions are measured as the average molar fraction over the 100 m path average NH_3, i.e. twice the 50 m distance to the retroreflectors. In doing so, we additionally assume the vertical NH_3 gradient to be horizontally homogeneous along the path. The potential impact of flow disruptions on the observed flux is difficult to quantify. However, we minimize the impact on the observations presented in this study, as we strictly filter for clear-sky summer condition where wind speeds are low. With less strict filter conditions however, these factors will likely influence the derived surface fluxes.

While these measurement uncertainties and proposed improvements could affect the inferred ammonia flux, the general observed pattern is still expected to remain. This pattern, where a large NH_3 gradient in the late afternoon results in high deposition, is not unique to our single-day Case, but is also found in the Averaged Summer Day observations.

4.2. The CLASS model

The CLASS mixed-layer model has proven an effective and inexpensive method to represent key CBL processes. The model was previously used to study the role of boundary layer dynamics on atmospheric chemistry by Vilà-Guerau de Arellano et al. (2011) and Ouwersloot et al. (2012). Vilà-Guerau de Arellano et al. (2011) additionally compared the model performance to the CBL-averaged values of the Dutch Atmospheric Large Eddy Simulation (DALES) model and concluded that the CLASS performance was reasonably similar to DALES. In this study, the CLASS model proves to be both powerful and flexible in its representation of processes involving (chemical) scalars, e.g. surface-atmosphere exchange, which can be either prescribed or parameterized.

This flexibility comes at the cost of simplifications. The main simplification is the description of atmospheric/tracer variables as a single value for the well-mixed CBL. As a result, the vertical gradient resulting from the gas-aerosol equilibrium of NH_3, which depends on temperature and relative humidity, is not captured by CLASS. These changes in equilibrium mixing ratios were shown to be important for ammonium nitrate mixing ratios (aan de Burgh et al., 2013). However, we again expect the impact on gaseous ammonia to be small due to the high temperatures. Furthermore, CLASS assumes horizontal homogeneity, which possibly does not hold true for ammonia, due to the nearby agricultural activity where very high NH_3 molar fractions are expected. The final major simplification of the model, the infinitely small inversion layer, is expected to only have a minor impact as well. This simplification mainly affects entrainment, which plays an important role in the morning growth of the CBL and is well represented by CLASS, as shown in Fig. 4a. The comparison by Vilà-Guerau de Arellano et al. (2011) also shows that CLASS performs well regarding entrainment and boundary layer growth when compared to the DALES model.

4.3. Representation of the NH_3 surface exchange

The process of surface-atmosphere exchange is represented following two different approaches: a prescribed NH_3 flux based on observations (Section 3.2) and a parameterized flux following DEPAC (Section 3.3). The ability to compare the performance of both approaches is a major advantage of the current strategy. It allows us to evaluate both the DOAS observed flux and the representation of the diurnal variability of the ammonia surface exchange by DEPAC.

DEPAC is well-established as a parameterization and is currently applied in Dutch operational air quality models OPS (Sauter et al., 2018) and LOTOS-EUROS (Schaap et al., 2008; Manders et al., 2017). These models are used in air quality predictions and policy making by the Dutch government, where the long term impact of ammonia on nitrogen deposition is the main focus. Therefore, these models are evaluated as such in literature and focus on yearly averages rather than subdaily scales as studied here. Despite the lack of emphasis on the subdaily time scales, which is the focus of this study, these validation studies still give us some indication of the performance of DEPAC under these prototypical convective conditions.

One of the few validation studies of DEPAC outside operational models is presented by Schrader et al. (2016). Here, the non-stomatal ammonia deposition path of DEPAC is compared to that of Massad et al. (2010) using observations from 5 locations in Europe, including the DOAS setup at Veenkampen. They showed that the performance of both parameterizations strongly differs per measurement site and an overall tendency for DEPAC to overestimate the non-stomatal ammonia deposition. However, only nighttime observations are used in this study as it is assumed that non-stomatal exchange is dominant during the night (Schrader et al., 2016). Furthermore, the observations used by Schrader et al. (2016) are taken over long time periods, e.g. 22 months at Veenkampen, and presented as daily averages. As a result, they mainly focused on the long term representation of NH_3 deposition, even though half-hourly observations are used.

Our study enables us to analyze how diurnal variations of meteorological variables influence the DEPAC model performance. In Section 3.3, we explain the mismatch between the DOAS observations and DEPAC, focusing on the parameterization of the stomatal compensation point, χ_{stom}. This stomatal compensation point is related to the emission potential (Γ_{stom}) following $\chi_{stom} = f(T)\Gamma_{stom}$, where $f(T)$ only depends on temperature as shown in Equation (16) of Appendix A. Wichink Kruit et al. (2010b) discuss that Γ_{stom} can be estimated from both bioassay measurements and micrometeorological observations. However, the latter method generally results in Γ_{stom} being a factor 3 higher compared to bioassay estimates in more polluted areas like Veenkampen (see Figure 9 from Wichink Kruit et al. (2010b)). This is supported by Loubet et al. (2002), who found stomatal compensation points for grass (*Lolium perenne*) up to 10 μg m^{-3} right after fertilization, based on bioassay measurements. DEPAC is based on micrometeorological measurements over unfertilized grass (*Lolium perenne*), but the $CLASS_{DEPAC}$ experiment estimates the daily average χ_{stom} to be 24 ppb, or 17 μg m^{-3}, shown in Fig. S3 of the Supplementary data in Appendix C. As a result, emission is found in the afternoon of the $CLASS_{DEPAC}$ experiment (5b). Such high values for χ_{stom} seem unrealistic, since the Veenkampen grassland site is unfertilized since 1979.

We do recognize that the DOAS observed fluxes are uncharacteristic over grassland in the Netherlands. High deposition up to -0.4 μg $m^{-2}s^{-1}$ has been observed before, but only in the early morning in relation to deposition onto dew droplets (Wichink Kruit et al., 2007). Focusing on the diurnal variability and these convective conditions, large afternoon NH_3 gradients, and the resulting deposition fluxes as presented in this study, have not been reported before over grassland and cannot be reproduced by the DEPAC parameterization. Loubet et al. (2012) did observe afternoon deposition of similar magnitude over tritical crop, where emission was expected. Their measurements could only partly be explained by high concentrations of certain acid gases (HNO_3 and SO_2) leading to high surface acidity. The large afternoon gradient presented here could not be explained by enhanced NH_3 deposition due to higher surface acidity (Appendix A), nor by observational uncertainties or gas-aerosol interactions (Section 4.1).

The results presented in this study on the diurnal variability of NH_3,

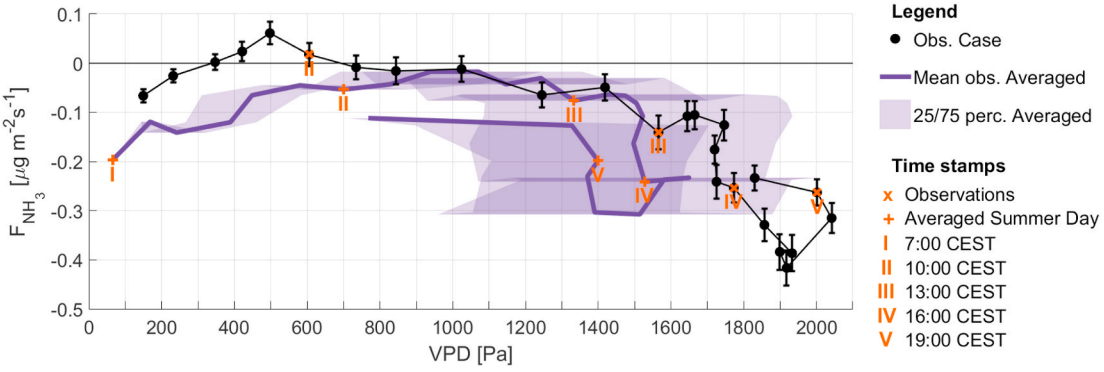

Fig. 7. The observed NH_3 flux against the water vapor pressure deficit plotted for the single-day Case (black) and the multi-day Averaged Summer Day (purple) with corresponding time stamps. Also shown are the uncertainty of NH_3 flux observations for the Case (errorbars) and the 25 and 75 percentile spread of the Averaged Summer Day observations for the VPD (purple shading). (For interpretation of the references to colour in this figure legend, the reader is referred to the Web version of this article.)

as well as differences in χ_{stom} estimations based on micrometeorological or bioassay measurements (Wichink Kruit et al., 2010b), indicate that the mechanisms behind the surface-atmosphere exchange of ammonia are not yet fully understood. This could have significant implications for approaches that incorporate the DEPAC module. It is relevant to note however, that these results on the diurnal variability cannot necessarily be applied directly to longer time scales, e.g. the seasonal variability which is reported on by Wichink Kruit et al. (2010b). We therefore recommend several follow-up studies, including validation of the DEPAC parameterization on longer time scales similar to Schrader et al. (2016), but now taking both the stomatal and the non-stomatal pathway into account. It would also be worthwhile to systematically study the performance of alternative parameterizations on the subdaily variability of the NH_3 flux. Finally, we believe systematic observations of the NH_3 vegetation-atmosphere exchange, focusing on the diurnal variability and covering different land use types, are required to allow for the development of more accurate parameterizations.

Related to the strong variability of temperature and therefore on vapor pressure deficit (VPD), new insights on the ammonia surface-atmosphere exchange could be gained by studying its relation to these meteorological variables. Fig. 7 shows observations of the NH_3 flux against the observed VPD. It seems that high deposition is related to the VPD increase in the afternoon. These observations show some similarities to the well-reported diurnal hysteresis between evapotranspiration and the VPD (Zhang et al., 2014; de Groot et al., 2019). Unfortunately, eddy covariance measurements of the water vapor and CO2 fluxes are not available for this study. Therefore, we are unable to further study the response of vegetation to the meteorological conditions and the potential relation to the ammonia surface exchange. However, these observations indicate that the ammonia surface-atmosphere exchange might be strongly regulated by the response of vegetation to diurnal meteorological conditions.

4.4. *Representation of NH_3 entrainment*

Observation and modeling studies showed that entrainment is as important as the surface exchange process in estimating the diurnal budget for moisture and CO_2 (Martin et al., 1988; Davis et al., 1994; Vilà-Guerau de Arellano et al., 2004; Casso-Torralba et al., 2008; van Heerwaarden et al., 2009). Furthermore, scientific studies on ammonium aerosols in the convective boundary layer have been conducted using large-eddy simulations (LES), with entrainment being explicitly resolved (Barbaro et al., 2015). However, the role of this process on the diurnal variability of atmospheric ammonia has not yet been studied.

We describe the entrainment flux following Equation (6), based on the modeled boundary layer dynamics (w_e) and the free tropospheric NH_3 molar fraction. Observations of free tropospheric ammonia are limited to tower observations and a handful of airborne campaigns, e.g. Nowak et al. (2010) and Tevlin et al. (2017). In the Netherlands, there have only been campaigns with ammonia measurements at the Cabauw meteorological tower up to 200 m, e.g. Erisman et al. (1988) and Dammers et al. (2017). While valuable, such tower observations are still within the convective boundary layer.

As observations are lacking, we perform a systematic estimation to find the best initial values for $NH_{3,\,FT}$ and the advection, as described in Section 2.6. This approach provides us with a robust method for a first estimate of the tropospheric NH_3 molar fraction, while testing the sensitivity of the ammonia budget to this variable. In doing so, $NH_{3,\,FT}$ is assumed to be constant with time and with height. This means that no NH_3 residual layer is simulated, even though radiosonde observations indicate the presence of a residual layer of potential temperature and specific humidity. However, as entrainment is dominant during the morning boundary layer growth, the estimated $NH_{3,\,FT}$ would effectively represent the NH_3 residual layer molar fraction. Therefore, the assumption of constant $NH_{3,\,FT}$ with height could lead to an overestimation of $NH_{3,\,FT}$ in the afternoon.

In order to better understand the role of entrainment on the budget, it would be convenient to observe NH_3 continuously at higher levels (> 100 m), similar to for example CO_2 and methane (CH_4) (Vermeulen et al., 2011). Our understanding of the role of entrainment in the diurnal variability of atmospheric ammonia could be further expanded by modeling studies where turbulent entrainment is explicitly resolved.

4.5. *Representation of NH_3 advection*

In boundary layer studies of atmospheric compounds, advection is generally considered a large-scale forcing term, e.g. for heat and moisture (Vilà-Guerau de Arellano et al., 2015; Ouwersloot et al., 2012) or CO2 (Vilà-Guerau de Arellano et al., 2004). For ammonia, it acts on smaller scales (100 m to several kilometers) as the high molar fraction over source areas decreases rapidly with distance (Fowler et al., 1998; Sommer et al., 2009; Shen et al., 2016). Depending on wind direction and source proximity, advection is shown to strongly increase NH_3 molar fractions (Loubet et al., 2012). Operational models do represent long-range advection, but are unable to capture this at sub-kilometer scales, as their typical spatial resolution ranges from 1 × 1 km to 50

× 50 km (Sauter et al., 2018; Schaap et al., 2008; Simpson et al., 2012). Attempts to capture and quantify short-range advection with observations has proven to be very challenging (Aubinet et al., 2010; Mauder et al., 2010). As a result, the representation of advection strongly differs in modeling studies (Vilà-Guerau de Arellano et al., 2004; 2011; aan de Burgh et al., 2012; Barbaro et al., 2015).

In this study, advection is the only term that is not based on observations. Ammonia advection is mainly driven by wind speed and direction, as well as the emission strength of nearby sources. The emission strength of a source is only rarely constant with time, e.g. emissions from organic wastes are related to changes in temperature (Pagans et al., 2006). We expect such changes to have a negligible impact on the advection at Veenkampen, as the small horizontal NH_3 gradient estimated from the prescribed advection indicates that the NH_3 emitted from nearby sources is already largely diluted when it reaches our site. Additionally, the wind direction during our Case is approximately constant and wind speeds are low. We therefore expect the assumption of constant advection to be valid as a first order estimate.

4.6. Representation of NH_3 chemical transformations

Chemical transformations of ammonia between the gas and aerosol phase only play a very small role in this budget study. We represent this process by coupling the ISORROPIA2 thermodynamic model to the CLASS model with a partitioning time (τ_p) of 30 min. ISORROPIA2 is used in the operational LOTOS-EUROS model and was used by aan de Burgh et al. (2013), Barbaro et al. (2015) and Guo et al. (2018). The partitioning time is very difficult to derive from in situ measurements, but the impact on ammonium nitrate formation was studied by aan de Burgh et al. (2013). They presented $\tau_p = 30$ min in their main results and the same time scale was later on used by Barbaro et al. (2015) and Guo et al. (2018).

The main source of uncertainty to our representation of the chemical transformation is a lack of observations on both the molar fraction of the relevant gaseous species and on particulate matter molar fractions and its composition. Such measurements, e.g. similar to Meng et al. (2018), could significantly improve our representation of this process. As it stands, we initialize CLASS based on the observations used by aan de Burgh et al. (2013), which were taken under similar fair-weather conditions and with ammonia molar fractions comparable to our Case. Due to the high temperatures and abundance of ammonia in our Case, we expect this uncertainty to only have a minor impact on the modeled ammonia budget.

Further sources of uncertainty come from the bulk model approach of the CLASS model as discussed in Section 4.2. The NH_3 gas-aerosol equilibrium moves towards gaseous NH_3 near the surface (high T and low RH) and towards aerosols near the top of the mixed-layer (low T and high RH). We expect that the aerosol molar fraction is slightly overestimated by using a bulk model approach, as the largest vertical gradient of the equilibrium molar fraction is found in the bottom half of the mixed-layer (aan de Burgh et al., 2013).

5. Conclusions

To analyze the diurnal variability of atmospheric ammonia (NH_3) over non-fertilized grassland, we perform a case study where we combine multiple observations with the CLASS conceptual boundary layer model. With the model, we disentangle and quantify the contributions of the four main processes governing the ammonia budget: surface-atmosphere exchange, entrainment, advection and chemical gas-aerosol transformations.

Our approach allows us to specifically addresses the role of the NH_3 surface-atmosphere exchange, by performing two numerical experiments where we vary the representation of this process. We first prescribe the surface flux based on observations and follow up by parameterizing the surface exchange. While both experiments perform similarly in reproducing the observed NH_3 molar fraction, we identify a mismatch between the DEPAC parameterized surface exchange and the observed flux. This leads to an unrealistic representation of the NH_3 budget for the second experiment, e.g. unrealistic high free tropospheric NH_3. The mismatch in the surface flux cannot be explained by the uncertainty of the NH_3 flux observations. This indicates a need for further research in the NH_3 surface-atmosphere exchange. Advancements such as improving the quantification of the stomatal compensation point through both micrometeorological and bioassay observations are recommended.

Based on the combination of the model and observations, our findings are summarized as follows:

- The mixed-layer model accurately reproduces the diurnal variability in the observed NH_3 molar fractions, when prescribing the observed surface flux.
- In the morning, boundary layer dynamics dominate the atmospheric NH_3 variability through entrainment.
- In the afternoon, the atmospheric NH_3 variability is controlled by processes acting on both non-local (advection) and local scales (surface-atmosphere exchange).
- Combining observations with the conceptual CLASS model has proven a powerful tool to both interpret observations and to analyze the performance of parameterizations to the diurnal variability of ammonia.

Data availability

Data are available from the corresponding author on request.

CRediT authorship contribution statement

R.B. Schulte: Conceptualization, Methodology, Software, Formal analysis, Investigation, Writing - original draft, Visualization. **M.C. van Zanten:** Writing - review & editing, Supervision, Funding acquisition. **S. Rutledge-Jonker:** Resources, Data curation, Writing - review & editing. **D.P.J. Swart:** Resources, Writing - review & editing. **R.J. Wichink Kruit:** Resources, Writing - review & editing. **M.C. Krol:** Software, Writing - review & editing. **W.A.J. van Pul:** Writing - review & editing, Funding acquisition. **J. Vilà-Guerau de Arellano:** Conceptualization, Methodology, Validation, Writing - review & editing, Supervision, Funding acquisition.

Declaration of competing interest

The authors declare that they have no known competing financial interests or personal relationships that could have appeared to influence the work reported in this paper.

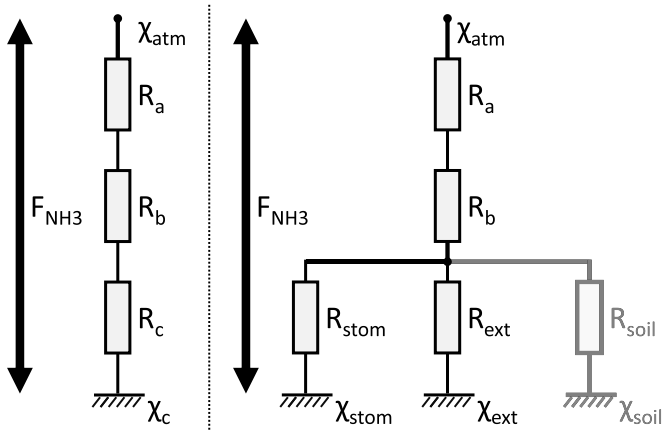

Fig. 8. A schematic representation of the DEPAC parameterization resistance model. A simplified representation with a combined canopy resistance and canopy compensation point is shown left. The complete resistance model with the separate deposition/emission paths is shown on the right. The soil path is shown grey as this path is assumed to be negligible for grassland, which is the focus of this paper.

Acknowledgments

We thank the Dutch National Institute of Public Health and the Environment (RIVM) air quality measurement team for their contributions to the ammonia molar fraction and deposition flux measurement, in particular René van der Hoff, Marty Haaima and Stijn Berkhout for their efforts in setting up and maintaining the DOAS instruments. We further want to thank Miranda Braam (RIVM) for her contributions to the ammonia data processing and interpretation. Finally, we thank Henk Klein Baltink (KNMI) for the LD40 ceilometer data. This research was financed by the Dutch National Institute of Public Health and the Environment (RIVM) within the framework of the Project 36.7: Monitoring of dry ammonia deposition, which is performed by order, and for the account, of the Dutch Ministry of Agriculture, Nature and Food Quality.

Appendix A. DEPAC parameterization for grassland

The DEPAC parameterization module is used in the Dutch OPS model and LOTOS-EUROS to calculate the dry deposition of ammonia and other acidifying acids. The module allows for 9 land use types, ranging from grass to coniferous forest and urban areas. Here, we describe the DEPAC modeling approach and the parameterization for grassland.

DEPAC describes multiple deposition pathways following the resistance modeling approach (van Zanten et al., 2010). Here, the deposition/emission flux results from a molar fraction difference ($\Delta\chi$) between the atmosphere (χ_{atm}) and the canopy at the surface (χ_c) and the resistance between them, i.e. $F = \Delta\chi/R$ equivalent to $I = V/R$ for electric circuits.

The atmosphere is connected to the surface by three resistances in series: two atmospheric resistances (R_a and R_b) and one canopy resistance (R_c), as shown on the left in Fig. 8. The ammonia surface flux (F_{sfc}) is calculated following Equation (10).

$$F_{sfc} = \frac{\chi_c - \chi_{atm}}{R_a + R_b + R_c} \tag{10}$$

Here, χ_{atm} is the atmospheric ammonia molar fraction, R represents the resistances and χ_c is the canopy compensation point, which represents the internal molar fraction of the canopy surface. Within the canopy, three deposition paths are described by the parameterization, as shown right in Fig. 8. The stomatal path (subscript *stom*) and the external leaf path (subscript *ext*) describe the atmosphere-vegetation exchange. The third pathway is to soils (subscript *soil*) and describes the atmosphere-soil exchange. The total canopy resistance R_c is calculated as three parallel resistances, following Equation (11).

$$\frac{1}{R_c} = \frac{1}{R_{stom}} + \frac{1}{R_{ext}} + \frac{1}{R_{soil}} \tag{11}$$

The canopy compensation point is the weighted average of the individual path compensation points, as shown in Equation (12).

$$\chi_c = \frac{R_c}{R_{stom}}\chi_{stom} + \frac{R_c}{R_{ext}}\chi_{ext} + \frac{R_c}{R_{soil}}\chi_{soil} \tag{12}$$

The first of the atmospheric resistances, the aerodynamic resistance (R_a), describes transport by turbulence and follows Equation (13).

$$R_a = \frac{1}{k\,u_*}\left[ln\left(\frac{z-d}{z_0}\right) - \Psi_H\left(\frac{z-d}{L}\right) + \Psi_H\left(\frac{z_0}{L}\right)\right] \tag{13}$$

Here, k is the Von Karman constant, u_* is the friction velocity, z is the height above the surface, d is the displacement height, z_0 is the roughness length, L is the Obukhov length and Ψ_H is the integrated stability function for heat of Paulson (1970) and Dyer (1974). The second atmospheric resistance is the quasi-laminar boundary layer resistance (R_b). Turbulent eddies do not penetrate this thin quasi-laminar boundary layer, which is in direct contact with the (canopy) surface. R_b is parameterized following to Equation (14).

$$R_b = \frac{2}{k\,u_*}\left(\frac{Sc}{Pr}\right)^{2/3} \tag{14}$$

Here, k is the Von Karman constant, u_* is the friction velocity, Sc is the Schmidt number and Pr is the Prandtl's number.

These three deposition pathways are shown left in Fig. 8. The stomatal path and the external leaf path describe the atmosphere-vegetation exchange. The soil pathway describes the atmosphere-soil exchange. For short and dense vegetation, like the grassland canopy used in this study, the single-layer or 'big-leaf' approach is applied and the soil pathway is assumed to be negligible.

Stomatal resistance (R_{stom}) is calculated following the A-g_s approach, as described in Section 2.5. The external leaf resistance (R_{ext}) in Equation (15) is based on the minimum external leaf surface resistance by Sutton and Fowler (1993) and observations at the Haarweg meteorological site by Wichink Kruit et al. (2010b).

$$R_{ext} = \frac{SAI_{Haarweg}}{SAI}\,\alpha\, exp\left(\frac{100 - RH}{\beta}\right) \tag{15}$$

Here, $SAI_{Haarweg}$ and SAI are the surface area index at the Haarweg and at the to be calculated location, RH is the relative humidity in % and α and β are parameterization constants with $\alpha = 2$ s m^{-1} and $\beta = 12\%$.

The compensation points of both paths are parameterized following Equation (16), based on the formulation of Nemitz et al. (2001) and Wichink Kruit et al. (2007).

$$\chi_{path} = \frac{2.75\ 10^{15}}{T_s + 273.15} exp\left(\frac{-1.04\ 10^{4}}{T_s + 273.15}\right)\Gamma_{path} \tag{16}$$

Here, T_s is the leaf surface temperature in °C and Γ is the dimensionless molar ratio between NH_4^+ and H^+, or emission potential. Subscript "*path*" indicates the deposition pathway, i.e. the stomatal or external leaf path. The two pathways differ only in their respective Γ parameterizations. For the stomatal deposition path, Γ_{stom} is solved following Equation (17), as described by Wichink Kruit et al. (2010b).

$$\Gamma_{stom} = 362\chi_{atm,\ 4\ m,\ long-term}\ 4.7exp(-0.071T_s) \tag{17}$$

Here, T_s is the leaf surface temperature in °C and $\chi_{atm,\ 4\ m,\ long-term}$ is the 'long-term' NH_3 molar fraction at 4 m height, for which we take the monthly average molar fraction. The external leaf deposition path is parameterized following Equation (18). The original formulation as described by van Zanten et al. (2010) is expanded with the codeposition factor for enhanced NH_3 deposition in the presence of SO_2, as described in Wichink Kruit et al. (2017).

$$\begin{aligned} \Gamma_{ext} &= F(\alpha_{SN})\left[1.84\ 10^{3}\chi_{atm,\ 4\ m}\ exp(-0.11T_s) - 850\right] \\ F(\alpha_{SN} &< 0.83) = 1.10 - 1.32\alpha_{SN} \\ F(\alpha_{SN} &\geq 0.83) = 0 \end{aligned} \tag{18}$$

Here, T_S is the leaf surface temperature in °C, $\chi_{atm,\ 4\ m}$ is the atmospheric molar fraction at 4 m height and α_{SN} is the molar ratio between annual average SO_2 and NH_3.

Appendix B. Experiment initialization

The $CLASS_{prescribed}$ and $CLASS_{DEPAC}$ numerical experiments are initialized following Table 2.

Table 2
Initialization of the $CLASS_{prescribed}$ and $CLASS_{DEPAC}$ numerical experiments.

Parameter	Symbol	Initial value	
	General		
Start time	t_0		05:30 UTC
End time	t_{end}		17:30 UTC
Step size	Δt		1 s
	Meteorological variables		
CBL height at t_0	$z_{0,\ 1}$		200 m
Transitional layer height at t_0	$z_{0,\ 2}$		410 m
Residual layer height at t_0	$z_{0,\ 3}$		700 m
Wind speed at t_0	u_0		2.0 m s^{-1}
Geostrophic wind speed at t_0	$u_{geo,\ 0}$		10.0 m s^{-1}
Flow divergence factor (subsidence)	*wsls*		3 10^{-6} s^{-1}
		Heat ($X = \theta$)	Moisture ($X = q$)
Initialization CBL at t_0	X_0	286 K	8.8 g kg^{-1}
Initialization inversion at t_0	ΔX	0.5 K	0.0 g kg^{-1}
Transition layer lapse rate	$\gamma_{X,\ 1}$	0.030 K m^{-1}	−0.005 g kg^{-1}m^{-1}
Residual layer lapse rate	$\gamma_{X,\ 2}$	0.005 K m^{-1}	−0.018 g kg^{-1}m^{-1}
Free troposphere lapse rate	$\gamma_{X,\ 3}$	0.010 K m^{-1}	−0.005 g kg^{-1}m^{-1}
	Surface properties		
Albedo	A		0.28
Leaf area index	LAI		3.0 (van Tiggelen et al., 2018)
Surface temperature at t_0	$T_{s,\ 0}$		289.5 K
Soil temperature top layer at t_0	$T_{soil,\ 0}$		292.0 K

(*continued on next page*)

Table 2 (*continued*)

Parameter	Symbol	Initial value	
Soil temperature deeper soil layer	T_2		282.0 K
Volumetric water content top soil layer at t_0	$w_{g,\,0}$		0.40 $m^3\ m^{-3}$
Volumetric water content deeper soil layer	w_2		0.72 $m^3\ m^{-3}$
Volumetric water content field capacity	w_{fc}		0.75 $m^3\ m^{-3}$
Saturated volumetric water content	w_{sat}		0.80 $m^3\ m^{-3}$
Wilting point	w_{wilt}		0.35 $m^3\ m^{-3}$
	Chemical species		
Chemical equilibrium time	τ		1800 s
Long term NH3 molar fraction	$\chi_{atm,\,long-term}$		15 ppb
		$CLASS_{prescribed}$	$CLASS_{DEPAC}$
NH_3 CBL at t_0	$NH_{3,\,0}$	27 ppb	27 ppb
NH_3 FT	$NH_{3,\,FT}$	0.00 ppb	11.0 ppb
NH_3 advection	ADV	0.72 10^{-3} ppb s^{-1}	0.04 10^{-3} ppb s^{-1}
HNO_3 CLB at t_0	$HNO_{3,\,0}$	3.5 ppb	3.5 ppb
HNO_3 FT	$HNO_{3,\,FT}$	1.0 ppb	1.0 ppb
H_2SO_4 at t_0	$H_2SO_{4,\,0}$	1.3 ppb	1.3 ppb
H_2SO_4 FT	$H_2SO_{4,\,FT}$	0.0 ppb	0.0 ppb

Appendix C. Supplementary data

Supplementary data to this article can be found online at https://doi.org/10.1016/j.atmosenv.2020.118153.

References

aan de Burgh, J.M.J., Henzing, J.S., Schaap, M., Morgan, W.T., van Heerwaarden, C.C., Weijers, E.P., Coe, H., Krol, M.C., 2012. Modelling the partitioning of ammonium nitrate in the convective boundary layer. Atmos. Chem. Phys. 12, 3005–3023. https://doi.org/10.5194/acp-12-3005-2012.

aan de Burgh, J.M.J., Ouwersloot, H.G., Vilà-Guerau de Arellano, J., Krol, M.C., 2013. A large-eddy simulation of the phase transition of ammonium nitrate in a convective boundary layer. J. Geophys. Res. Atmos. 118, 826–836. https://doi.org/10.1002/jgrd.50161.

Aubinet, M., Feigenwinter, C., Heinesch, B., Bernhofer, C., Canepa, E., Lindroth, A., Montagnani, L., Rebmann, C., Sedlak, P., van Gorsel, E., 2010. Direct advection measurements do not help to solve the night-time CO_2 closure problem: evidence from three different forests. Agric. For. Meteorol. 150, 655–664. https://doi.org/10.1016/j.agrformet.2010.01.016.

Barbaro, E., Krol, M.C., Vilà-Guerau de Arellano, J., 2015. Numerical simulation of the interaction between ammonium nitrate aerosol and convective boundary-layer dynamics. Atmos. Environ. 105, 202–211. https://doi.org/10.1016/j.atmosenv.2015.01.048.

Beljaars, A.C.M., Holtslag, A.A.M., 1991. Flux parameterization over land surfaces for atmospheric models. J. Appl. Meteorol. 30, 327–341. https://doi.org/10.1175/1520-0450(1991)030%3C0327:fpolsf%3E2.0.co;2.

Bobbink, R., Hornung, M., Roelofs, J.G.M., 2003. The effects of air-borne nitrogen pollutants on species diversity in natural and semi-natural european vegetation. J. Ecol. 86, 717–738. https://doi.org/10.1046/j.1365-2745.1998.8650717.x.

von Bobrutzki, K., Braban, C.F., Famulari, D., Jones, S.K., Blackall, T., Smith, T.E.L., Blom, M., Coe, H., Gallagher, M., Ghalaieny, M., McGillen, M.R., Percival, C.J., Whitehead, J.D., Ellis, R., Murphy, J., Mohacsi, A., Pogany, A., Junninen, H., Rantanen, S., Sutton, M.A., Nemitz, E., 2010. Field inter-comparison of eleven atmospheric ammonia measurement techniques. Atmos. Meas. Tech. 3, 91–112. https://doi.org/10.5194/amt-3-91-2010.

Calders, K., Schenkels, T., Bartholomeus, H., Armston, J., Verbesselt, J., Herold, M., 2015. Monitoring spring phenology with high temporal resolution terrestrial LiDAR measurements. Agric. For. Meteorol. 203, 158–168. https://doi.org/10.1016/j.agrformet.2015.01.009.

Casso-Torralba, P., Vilà-Guerau de Arellano, J., Bosveld, F., Soler, M.R., Vermeulen, A., Werner, C., Moors, E., 2008. Diurnal and vertical variability of the sensible heat and carbon dioxide budgets in the atmospheric surface layer. J. Geophys. Res.: Atmos. 113 https://doi.org/10.1029/2007JD009583.

Dammers, E., Schaap, M., Haaima, M., Palm, M., Wichink Kruit, R.J, Volten, H., Hensen, A., Swart, D.P.J., Erisman, J.W., 2017. Measuring atmospheric ammonia with remote sensing campaign: Part 1 – characterisation of vertical ammonia concentration profile in the centre of The Netherlands. Atmos. Environ. 169, 97–112. https://doi.org/10.1016/j.atmosenv.2017.08.067.

Davis, K.J., Lenschow, D.H., Zimmerman, P.R., 1994. Biogenic nonmethane hydrocarbon emissions estimated from tethered balloon observations. J. Geophys. Res.: Atmos. 99, 25587–25598. https://doi.org/10.1029/94JD02009.

Dyer, A.J., 1974. A review of flux-profile relationships. Boundary-Layer Meteorol. 7, 363–372. https://doi.org/10.1007/BF00240838.

Dyer, A.J., Hicks, B.B., 1970. Flux-gradient relationships in the constant flux layer. Q. J. R. Meteorol. Soc. 96, 715–721. https://doi.org/10.1002/qj.49709641012.

Erisman, J.W., Vermetten, A.W.M., Asman, W.A.H., Waijers-Ijpelaan, A., Slanina, J., 1988. Vertical distribution of gases and aerosols: the behaviour of ammonia and related components in the lower atmosphere. Atmos. Environ. 22, 1153–1160. https://doi.org/10.1016/0004-6981(88)90345-9, 1967.

Erisman, J.W., Bleeker, A., Galloway, J., Sutton, M.S., 2007. Reduced nitrogen in ecology and the environment. Environ. Pollut. 150, 140–149. https://doi.org/10.1016/j.envpol.2007.06.033.

Erisman, J.W., Galloway, J.N., Seitzinger, S., Bleeker, A., Dise, N.B., Petrescu, R.A.M., Leach, A.M., de Vries, W., 2013. Consequences of human modification of the global nitrogen cycle. Phil. Trans. Biol. Sci. 368, 20130116. https://doi.org/10.1098/rstb.2013.0116.

Farquhar, G.D., Firth, P.M., Wetselaar, R., Weir, B., 1980. On the gaseous exchange of ammonia between leaves and the environment: determination of the ammonia compensation point. Plant Physiol. 66, 710–714. https://doi.org/10.1104/pp.66.4.710.

Fountoukis, C., Nenes, A., 2007. Isorropia II: a computationally efficient thermodynamic equilibrium model for K^+-Ca^{2+}-Mg^{2+}-$NH4^+$-Na^+-$SO4^{2-}$-$NO3^-$-Cl^--H2O aerosols. Atmos. Chem. Phys. 7, 4639–4659. https://doi.org/10.5194/acp-7-4639-2007.

Fowler, D., Pitcairn, C.E.R., Sutton, M.A., Flechard, C., Loubet, B., Coyle, M., Munro, R. C., 1998. The mass budget of atmospheric ammonia in woodland within 1 km of livestock buildings. Environ. Pollut. 102, 343–348. https://doi.org/10.1016/S0269-7491(98)80053-5.

de Groot, G.E., Vilà-Guerau de Arellano, J., de Roode, S.R., Coenders-Gerrits, A.M.J., van de Wiel, B.J.H., 2019. Evaporation hysteresis over vegetation: the impact of surface processes and boundary layer dynamics. Master's thesis. Delft University of Technology, the Netherlands. http://resolver.tudelft.nl/uuid:8284f137-2c64-48ab-ba8d-bf099d70c70c.

Guo, H., Otjes, R., Schlag, P., Kiendler-Scharr, A., Nenes, A., Weber, R.J., 2018. Effectiveness of ammonia reduction on control of fine particle nitrate. Atmos. Chem. Phys. 18, 12241–12256. https://doi.org/10.5194/acp-18-12241-2018.

van Heerwaarden, C.C., Vilà-Guerau de Arellano, J., Moene, A.F., Holtslag, A.A.M., 2009. Interactions between dry-air entrainment, surface evaporation and convective boundary-layer development. Q. J. R. Meteorol. Soc. 135, 1277–1291. https://doi.org/10.1002/qj.431.

Izett, J.G., van de Wiel, B.J.H., Baas, P., Bosveld, F.C., 2018. Understanding and reducing false alarms in observational fog prediction. Boundary-Layer Meteorol. 169, 347–372. https://doi.org/10.1007/s10546-018-0374-2.

Loubet, B., Milford, C., Hill, P.W., Tang, Y.S., Cellier, P., Sutton, M.A., 2002. Seasonal variability of apoplastic $NH4^+$ and pH in an intensively managed grassland. Plant Soil 238, 97–110. https://doi.org/10.1023/A:1014208926195.

Loubet, B., Decuq, C., Personne, E., Massad, R.S., Flechard, C., Fanucci, O., Mascher, N., Gueudet, J.C., Masson, S., Durand, B., Genermont, S., Fauvel, Y., Cellier, P., 2012. Investigating the stomatal, cuticular and soil ammonia fluxes over a growing tritical crop under high acidic loads. Biogeosciences 9, 1537–1552. https://doi.org/10.5194/bg-9-1537-2012.

Manders, A.M.M., Builtjes, P.J.H., Curier, L., Denier van der Gon, H.A.C., Hendriks, C., Jonkers, S., Kranenburg, R., Kuenen, J.J.P., Segers, A.J., Timmermans, R.M.A., Visschedijk, A.J.H., Wichink Kruit, R.J., van Pul, W.A.J., Sauter, F.J., van der Swaluw, E., Swart, D.P.J., Douros, J., Eskes, H., van Meijgaard, E., van Ulft, B., van

Velthoven, P., Banzhaf, S., Mues, A.C., Stern, R., Fu, G., Lu, S., Heemink, A., van Velzen, N., Schaap, M., 2017. Curriculum vitae of the LOTOS-EUROS (v2.0) chemistry transport model. Geosci. Model Dev. (GMD) 10, 4145–4173. https://doi.org/10.5194/gmd-10-4145-2017.

Martin, C.L., Fitzjarrald, D., Garstang, M., Oliveira, A.P., Greco, S., Browell, E., 1988. Structure and growth of the mixing layer over the amazon rain forest. J. Geophys. Res. Atmos. 93 https://doi.org/10.1029/JD093iD02p01361.

Massad, R.S., Nemitz, E., Sutton, M.A., 2010. Review and parameterisation of bi-directional ammonia exchange between vegetation and the atmosphere. Atmos. Chem. Phys. 10, 10359–10386. https://doi.org/10.5194/acp-10-10359-2010.

Matthias, V., Arndt, J.A., Aulinger, A., Bieser, J., Denier van der Gon, H., Kranenburg, R., Kuenen, J., Neumann, D., Pouliot, G., Quante, M., 2018. Modeling emissions for three-dimensional atmospheric chemistry transport models. J. Air Waste Manag. Assoc. 68, 763–800. https://doi.org/10.1080/10962247.2018.1424057.

Mauder, M., Desjardins, R.L., Pattey, E., Worth, D., 2010. An attempt to close the daytime surface energy balance using spatially-averaged flux measurements. Boundary-Layer Meteorol. 136, 175–191. https://doi.org/10.1007/s10546-010-9497-9.

Meng, Z., Xu, X., Lin, W., Ge, B., Xie, Y., Song, B., Jia, S., Zhang, R., Peng, W., Wang, Y., Cheng, H., Yang, W., Zhao, H., 2018. Role of ambient ammonia in particulate ammonium formation at a rural site in the North China Plain. Atmos. Chem. Phys. 18, 167–184. https://doi.org/10.5194/acp-18-167-2018.

Nemitz, E., Milford, C., Sutton, M.A., 2001. A two-layer canopy compensation point model for describing bi-directional biosphere-atmosphere exchange of ammonia. Q. J. R. Meteorol. Soc. 127, 815–833. https://doi.org/10.1002/qj.49712757306.

Nemitz, E., Sutton, M.A., Wyers, G.P., Otjes, R.P., Mennen, M.G., van Putten, E.M., Gallagher, M.W., 2004. Gas-particle interactions above a Dutch heathland: II. Concentrations and surface exchange fluxes of atmospheric particles. Atmos. Chem. Phys. 4, 1007–1024. https://doi.org/10.5194/acp-4-1007-2004.

Nowak, J.B., Neuman, J.A., Bahreini, R., Brock, C.A., Middlebrook, A.M., Wollny, A.G., Holloway, J.S., Peischl, J., Ryerson, T.B., Fehsenfeld, F.C., 2010. Airborne observations of ammonia and ammonium nitrate formation over Houston, Texas. J. Geophys. Res.: Atmos. 115 https://doi.org/10.1029/2010JD014195.

Ouwersloot, H.G., Vilà-Guerau de Arellano, J., Nölscher, A.C., Krol, M.C., Ganzeveld, L. N., Breitenberger, C., Mammarella, I., Williams, J., Lelieveld, J., 2012. Characterization of a boreal convective boundary layer and its impact on atmospheric chemistry during HUMPPA-COPEC-2010. Atmos. Chem. Phys. 12, 9335–9353. https://doi.org/10.5194/acp-12-9335-2012.

Pagans, E., Barrena, R., Font, X., Sánchez, A., 2006. Ammonia emissions from the composting of different organic wastes. dependency on process temperature. Chemosphere 62, 1534–1542. https://doi.org/10.1016/j.chemosphere.2005.06.044.

Paulson, C.A., 1970. The mathematical representation of wind speed and temperature profiles in the unstable atmospheric surface layer. J. Appl. Meteorol. 9, 857–861. https://doi.org/10.1175/1520-0450(1970)009%3C0857:tmrows%3E2.0.co;2.

Ronda, R.J., de Bruin, H.A.R., Holtslag, A.A.M., 2001. Representation of the canopy conductance in modeling the surface energy budget for low vegetation. J. Appl. Meteorol. 40, 1431–1444. https://doi.org/10.1175/1520-0450(2001)040<1431:ROTCCI>2.0.CO;2.

Sauter, F., van Zanten, M., van der Swaluw, E., Aben, J., de Leeuw, F., van Jaarsveld, H., 2018. The OPS-model: description of OPS 4.5.2. Technical Report. National Institute for Public Health and the Environment (RIVM. https://www.rivm.nl/media/ops/OPS-model.pdf.

Schaap, M., Timmermans, R.M.A., Roemer, M., Boersen, G.A.C., Builtjes, P.J.H., Sauter, F.J., Velders, G.J.M., Beck, J.P., 2008. The LOTOS–EUROS model: description, validation and latest developments. Int. J. Environ. Pollut. 32, 270–290. https://doi.org/10.1504/IJEP.2008.017106.

Schrader, F., Brüummer, C., Flechard, C.R., Wichink Kruit, R.J., van Zanten, M.C., Zöll, U., Hensen, A., Erisman, J.W., 2016. Non-stomatal exchange in ammonia dry deposition models: comparison of two state-of-the-art approaches. Atmos. Chem. Phys. 16, 13417–13430. https://doi.org/10.5194/acp-16-13417-2016.

Schrader, F., Schaap, M., Zöll, U., Kranenburg, R., Brümmer, C., 2018. The hidden cost of using low-resolution concentration data in the estimation of NH3 dry deposition fluxes. Sci. Rep. 8 https://doi.org/10.1038/s41598-017-18021-6.

Shen, J., Chen, D., Bai, M., Sun, J., Coates, T., Lam, S.K., Li, Y., 2016. Ammonia deposition in the neighbourhood of an intensive cattle feedlot in Victoria, Australia. Sci. Rep. 6, 2045–2322. https://doi.org/10.1038/srep32793.

Simpson, D., Benedictow, A., Berge, H., Bergström, R., Emberson, L.D., Fagerli, H., Flechard, C.R., Hayman, G.D., Gauss, M., Jonson, J.E., Jenkin, M.E., Nyíri, A., Richter, C., Semeena, V.S., Tsyro, S., Tuovinen, J.P., Valdebenito, ., Wind, P., 2012. The EMEP MSC-W chemical transport model - technical description. Atmos. Chem. Phys. 12, 7825–7865. https://doi.org/10.5194/acp-12-7825-2012.

Sommer, S.G., Østergård, H.S., Løfstrøm, P., Andersen, H.V., Jensen, L.S., 2009. Validation of model calculation of ammonia deposition in the neighbourhood of a poultry farm using measured NH3 concentrations and N deposition. Atmos. Environ. 43, 915–920. https://doi.org/10.1016/j.atmosenv.2008.10.045.

Stull, R., 1988. An Introduction to Boundary Layer Meteorology. Kluwer Academic Publishers.

Sutton, M., Fowler, D., 1993. A model for inferring bi-directional fluxes ofammonia over plant canopies. In: Proceedings of the WMO Conference on the Measurement and Modelling of Atmospheric Composition Changes Including Pollution Transport. WMO, Geneva, pp. 179–182.

Sutton, M.A., Schjørring, J.K., Wyers, G.P., Duyzer, J.H., Ineson, P., Powlson, D.S., Fowler, D., Jenkinson, D.S., Monteith, J.L., Unsworth, M.H., 1995. Plan—atmosphere exchange of ammonia. Philos. Trans. R. Soc. London, Ser. A: Phys. Eng. Sci. 351, 261–278. https://doi.org/10.1098/rsta.1995.0033.

Sutton, M.A., Erisman, J.W., Dentener, F., Möller, D., 2008. Ammonia in the environment: from ancient times to the present. Environ. Pollut. 156, 583–604. https://doi.org/10.1016/j.envpol.2008.03.013.

Tevlin, A.G., Li, Y., Collett, J.L., McDuffie, E.E., Fischer, E.V., Murphy, J.G., 2017. Tall tower vertical profiles and diurnal trends of ammonia in the Colorado front range. J. Geophys. Res.: Atmos. 122 (12) https://doi.org/10.1002/2017JD026534, 468–12,487.

van Tiggelen, M., de Roode, S.R., Siebesma, A., van de Wiel, B., 2018. Towards improving the land-surface-atmosphere coupling in the Dutch Atmospheric Large-Eddy Simulation model (DALES). Delft University of Technology, the Netherlands. Master's thesis. http://resolver.tudelft.nl/uuid:bbe384d1-3f40-487a-b1a6-7ce34438f2db.

Velders, G., Aben, J., Geilenkirchen, G., den Hollander, H., Noordijk, H., de Vries, W., Wesseling, J., van Zanten, M., 2014. Grootschalige concentratie- en depositiekaarten Nederland. Rapportage 2014. Technical Report 680363002. National Institute for Public Health and the Environment (RIVM). https://www.rivm.nl/bibliotheek/rapporten/680363002.pdf.

Vermeulen, A.T., Hensen, A., Popa, M.E., Bulk, W.C.M., Jongejan, P.A.C., 2011. Greenhouse gas observations from Cabauw tall tower (1992-2010). Atmos. Meas. Tech. 4, 617. https://doi.org/10.5194/amt-4-617-2011.

Vilà-Guerau de Arellano, J., Duynkerke, P.G., Builtjes, P.J.H., 1993. The divergence of the turbulent diffusion flux due to chemical reactions in the surface layer: NO-O3-NO2 system. Tellus B 45, 23–33. https://doi.org/10.1034/j.1600-0889.1993.00002.x.

Vilà-Guerau de Arellano, J., Gioli, B., Miglietta, F., Jonker, H.J.J., Klein Baltink, H., Hutjes, R.W.A., Holtslag, A.A.M., 2004. Entrainment process of carbon dioxide in the atmospheric boundary layer. J. Geophys. Res.: Atmos. 109 https://doi.org/10.1029/2004JD004725.

Vilà-Guerau de Arellano, J., Patton, E.G., Karl, T., van den Dries, K., Barth, M.C., Orlando, J.J., 2011. The role of boundary layer dynamics on the diurnal evolution of isoprene and the hydroxyl radical over tropical forests. J. Geophys. Res.: Atmos. 116 https://doi.org/10.1029/2010JD014857.

Vilà-Guerau de Arellano, J., van Heerwaarden, C.C., van Stratum, B.J.H., van den Dries, K., 2015. A. tmospheric boundary layer: integrating air chemistry and land interactions. Cambridge University Press. https://doi.org/10.1017/CBO9781316117422.

Volten, H., Bergwerff, J.B., Haaima, M., Lolkema, D.E., Berkhout, A.J.C., van der Hoff, G. R., Potma, C.J.M., Wichink Kruit, R.J., van Pul, W.A.J., Swart, D.P.J., 2012a. Two instruments based on differential optical absorption spectroscopy (DOAS) to measure accurate ammonia concentrations in the atmosphere. Atmos. Meas. Tech. 5, 413–427. https://doi.org/10.5194/amt-5-413-2012.

Volten, H., Haaima, M., Swart, D.P.J., van Zanten, M.C., van Pul, W.A.J., 2012b. Ammonia exchange measured over a corn field in 2010. Technical Report 680180003. National Institute for Public Health and the Environment (RIVM). https://www.rivm.nl/bibliotheek/rapporten/680180003.pdf.

Whitehead, J.D., Twigg, M., Famulari, D., Nemitz, E., Sutton, M.A., Gallagher, M.W., Fowler, D., 2008. Evaluation of laser absorption spectroscopic techniques for eddy covariance flux measurements of ammonia. Environ. Sci. Technol. 42, 2041–2046. https://doi.org/10.1021/es071596u.

Wichink Kruit, R.J., van Pul, W.A.J., 2018. Ontwikkelingen in de stikstofdepositie. Briefrapport 2018-0117. National Institute for Public Health and the Environment (RIVM). https://doi.org/10.21945/RIVM-2018-0117.

Wichink Kruit, R.J., van Pul, W.A.J., Otjes, R.P., Hofschreuder, P., Jacobs, A.F.G., Holtslag, A.A.M., 2007. Ammonia fluxes and derived canopy compensation points over non-fertilized agricultural grassland in The Netherlands using the new GRadient Ammonia - high Accuracy - Monitoring (GRAHAM). Atmos. Environ. 41, 1275–1287. https://doi.org/10.1016/j.atmosenv.2006.09.039.

Wichink Kruit, R.J., Haaima, M., Swart, D.P.J., van Zanten, M.C., van Pul, W.A.J., 2010a. Ammonia exchange measurements over a corn field in Lelystad, The Netherlands in 2009. Technical Report 680180002. National Institute for Public Health and the Environment (RIVM). https://www.rivm.nl/bibliotheek/rapporten/680180002.pdf.

Wichink Kruit, R.J., van Pul, W.A.J., Sauter, F.J., van den Broek, M.E.N., Sutton, M.A., Krol, M., Holtslag, A.A.M., 2010b. Modeling the surface–atmosphere exchange of ammonia. Atmos. Environ. 44, 945–957. https://doi.org/10.1016/j.atmosenv.2009.11.049.

Wichink Kruit, R.J., Aben, J., de Vries, W., Sauter, F., van der Swaluw, E., van Zanten, M. C., van Pul, W.A.J., 2017. Modelling trends in ammonia in The Netherlands over the period 1990–2014. Atmos. Environ. 154, 20–30. https://doi.org/10.1016/j.atmosenv.2017.01.031.

van Zanten, M.C., Sauter, F.J., Wichink Kruit, R.J., van Jaarsveld, J.A., van Pul, W.A.J., 2010. Description of the DEPAC module: dry deposition modelling with DEPAC-GCN2010. National Institute for Public Health and the Environment. Technical Report 680180001. https://www.rivm.nl/bibliotheek/rapporten/680180001.pdf (RIVM). URL:

Zhang, Q., Manzoni, S., Katul, G., Porporato, A., Yang, D., 2014. The hysteretic evapotranspiration – vapor pressure deficit relation. J. Geophys. Res.: Biogeosciences 119, 125–140. https://doi.org/10.1002/2013JG002484.